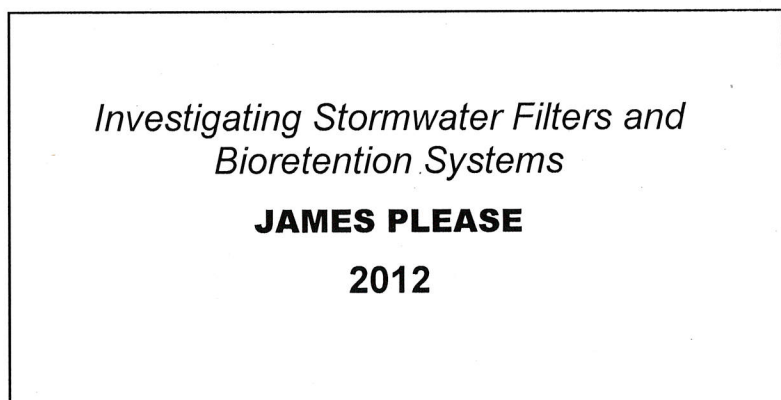


I certify that all material in this thesis that is not my own work has been identified and that no material has been included for which a degree has previously been conferred on me.

Signed.....



Micro-Scale Experimental Investigation to Determine the Pore Geometries of the Hydro Filterra™ Bioretention Media with Experimental Validation to Computational Models Using Additive Layer Manufacturing Techniques

For Group Project:

Investigating Stormwater Filters and Bioretention Systems

A Study on the Filterra™ System Manufactured by Hydro-International Ltd. (UK)

Individual Report – I2



James C Please

CANDIDATE NUMBER

580010419

May 2012

Supervisor: Dr Gavin Tabor

Abstract

Bioretention systems use different grades of specifically designed filter media and the use of biological processes to remove pollutants from stormwater, whilst regulating flow. Implemented at the entry to the urban drainage system, they are an effective way to manage surface water pollutants in both a sustainable and energy-efficient manner. Using recent developments in X-Ray tomography and micro-CT technology, this report examines the filtration matrix within *Hydro Filterra™* bioretention systems from microscopic investigation and examination of the 3D porous soil/root structure. Experimental and theoretical findings are compared with results from macro-scale tests to investigate variance in hydraulic properties, and look at the ways in which microscopic quantification of pore space geometries compare with properties inferred from hydraulic tests.

Keywords

Micro-CT, Porous Media, Attenuation Coefficients, Packed Beds, Soil Microarchitecture

Acknowledgements

Thanks must be given to;

- **Dr. Lesley Wears** (*University of Exeter*). For her time and resources given to provide micro-CT scans and continued support throughout the project.
 - **Ed James** (*C.A.L.M Exeter*). Whose help with 3D modelling of scan data, and willingness to assist with new applications of additive layer manufacturing have been fundamental in the success of the testing phase of the project.
 - **Daniel Jarman** (*Hydro Int. (UK)*). For continued support and industrial feedback, provision of resources, case study details and the collaboration for a very successful field trip.
 - **Dr. Matthew Baker** (*Innovation Centre, University of Exeter*). Whose help with the testing has been invaluable, and provision of experimental equipment has helped enormously.
 - **Dr. Gavin Tabor** (*University of Exeter*) – For support, assistance, guidance and academic input throughout.
 - **Roger Perrett** (*University of Exeter*) – For provision of resources and laboratory space.
-

Contents

Abstract.....	i
Keywords	i
Acknowledgements.....	ii
Table of Figures	
1. Introduction.....	1
1.1. Bioretention Systems	1
1.2. An Introduction to Porous Media	2
1.3. Filterra™ Filter Media.....	3
1.4. Case Study	3
2. Soil Structure	4
2.1. Porosity	4
2.2. Particle Size Distribution.....	5
2.3. Permeability/Hydraulic Conductivity	5
2.3.1. Darcy's Law	6
2.3.2. Navier-Stokes	7
2.3.3. Hazen's Law.....	9
2.3.4. Packed Bed Theory.....	9
3. Imaging Techniques	10
3.1. X-Ray Computed Tomography (XCT).....	11
3.1.1. Principles.....	11
3.1.2. Micro-CT.....	12
3.1.3. Considerations.....	13
3.2. Alternative Techniques.....	14
3.3. Micro C-T Application	14
4. Experimental Project Management.....	15
4.1. Group Management.....	15
4.2. Individual Management.....	15
5. Methodology.....	18
5.1. Phase 2: Scanning Initial stages and Experimental Protocol Design.....	18
5.1.1. Phase 2.1 – Modification of Experimental Technique.....	18

5.1.2. Phase 2.2 – Initial Scans.....	19
5.2. Phase 3: Scanning of filter medium sample extracted from macro-scale permeameter test	20
5.3. Phase 4: Scanning of filter medium sample extracted from case study system.....	21
5.4. Phase 5: Sieve Testing and PSD investigation of the various filter medium samples	21
5.5. Phase 6: 3D Model construction and Rapid Prototype of scanned profile.....	22
5.6. Phase 7: Flow tests on Rapid Prototype sample.....	23
5.7. Phase 9: Attenuation investigation	24
5.8. Health and Safety Considerations.....	25
6. Results & Discussion.....	25
6.1. Phase 2:	25
6.2. Phase 3/4:.....	27
6.3. Phase 5:.....	30
6.4. Phase 6:	31
6.5. Phase 7:.....	32
6.6. Phase 8:.....	34
6.7. Phase 9	36
7. Conclusion.....	38
8. Recommendation of Future Work.....	39
9. Project Review.....	40
References	
Appendices.....	

Table of Figures

Figure 1 (Hydro, 2011) <i>Diagram representing Filterra™ process</i>	2
Figure 2 – Darcy’s experimental investigation of permeability.....	6
Figure 3 (Gregory, et al., 2003) – Simplified layout of a micro-CT scanner.....	13
Figure 4 - Flow of Experimental Project Management.....	17
Figure 5 – Images of the ‘X-Tek Benchtop CT’ micro-CT Machine (X-Tek Xray Systems, 2006)	18
Figure 6 - Scaling of 3D model and Extraction of region for Rapid Prototyping	22
Figure 7 - Experimental Setup for Flow Tests	24
Figure 8 - Scan images for 'Fine-Gravel' (sample #1) from initial scan samples	26
Figure 9 - Cutaway view of 3D volume reconstruction - 'Hydro Lab' sample	27
Figure 10 - Cutaway view of 3D volume reconstruction - 'Case Study' sample	27
Figure 11 - AC Histogram and 2D Images used simultaneously for pore identification – 'Case Study' Sample	28
Figure 12 - Particle Size Distribution for 3 sample media	30
Figure 13 - Final models created using Additive Layer Manufacturing	31
Figure 14 - Graph of Pressure drop per length VS Superficial Velocity and Particle Reynolds Number - For ALM 'Case Study' Sample.....	32
Figure 15 - Graph of Pressure drop per length VS Redp for 'ALM filter media sample' and 'packed bed sample' (log scale).....	33
Figure 16 - Graph of dimensionless pressure drop VS particle Reynolds number for ALM sample and packed bed sample, with theoretical trendlines based on Ergun and Eisfield & Scnitzlein equations	34
Figure 17 - Graph comparing pressure drop/superficial velocity results for Darcy Forscheimer, CFD models, and ALM Model Flow tests.....	35
Figure 18 - Greyscale Attenuation Histograms for scanned samples	36
Figure 19 - Normalised Greyscale Attenuation Histograms for scanned samples.....	36
Figure 20 - 3D Volume Rendered image of Hydro Sample following Phase Segmentation....	38

1. Introduction

In 2012, the UK will see the introduction of the Sustainable Urban Drainage Systems (SUDS) legislation, aimed at increasing the focus on water purification and treatment within the urban drainage network. For a number of years, with an increasing level of urban expansion (European Environment Agency, 2006), the need to address the issue of storm waste water and urban runoff has become increasingly evident. In non-urban, natural areas, storm water and ground water runoff passes through the water cycle in a standard manner, with natural irrigation and filtering. Organic content is filtered and deposited naturally, and the cycle for the most part remains self-sustained. In the case of urban drainage however, the need to control high flow rates and more importantly the removal of non-organic pollutants must be addressed prior to the water re-entering the natural water cycle. Existing urban drainage networks typically address this problem through the use of irrigation networks that feed large scale water treatment plants. This approach to stormwater management is, and has been, functional throughout history; however with a growing awareness of sustainable, environmentally friendly alternatives within infrastructure, more effort is being made to adopt an approach where waste/stormwater is controlled closer to the entry to the sewerage system. At entry, efficient methods can be implemented to manage both pollutant and flow levels. Many smaller scale biological and/or mechanical processes including bioretention systems are able to clean and regulate surface run-off, thus reducing load and operating requirements of large scale water treatment works downstream.

1.1. Bioretention Systems

Most bioretention systems are designed with two overall aims:

- Flow control (stormwater management)
- Pollutant Removal (micro and macro-scale)

Some systems are designed specifically for the regulation of either pollutant removal or flow control. Pollutant removal can be divided into two categories; Biologically Active Filtration, where biological uptake and vegetation/root processes contribute to adsorption through active filtration, and Biologically Inactive Filtration, where inert filtration is carried out through physical processes as in sand filters. In the case of the system discussed in this paper, these aims are both addressed through an integrated system comprising a specially designed multi-layer filter media, and a plant/root system. Whilst the filter media is able to control flow and remove macro-scale pollutants from the system, the soil/root system employs root absorption capabilities to remove micro-scale pollutants and contaminants through biologically active means. Conventional bioretention systems operate under slow flow-rate conditions, however thanks to an efficient design that utilises various filtration methods, the Filterra™ system can provide pollutant removal at high flow rates, allowing it to not only operate as a filtration mechanism but also as a storm water control device.

An integrated system, as shown in Figure 1, presents a number of challenges in both design and understanding. One area of investigation is removal of pollutants, governed primarily by the biological processes in the plant/root system. The company *Hydro International Ltd.* have conducted extensive research into the pollutant removal capabilities of the system, with statistics obtained for chemical uptake in a variety of conditions by independent researchers (Geosyntec Consultants, Herrera Consultants, 2010). The other area of investigation surrounds the filter media, and its ability to regulate flow through the system. In order to implement the bioretention system in the urban drainage network, an extensive understanding of the flow properties of the system is required. Flow through the specifically designed porous

media is the primary area of investigation within this project. Forming part of a larger group project, this individual report shall be concentrating on characterising the porous filter media. Through theoretical and experimental methods the project investigates the geometric aspects of the pore system on a micro-scale, how this affects hydraulic properties on a macro-scale, and how experimental behaviour compares with computational models. The work carried out throughout this project has been conducted in collaboration with other group members, further details of related work can be found in 'Investigating Stormwater Filters and Bioretention Systems' (Begley, et al., 2012).

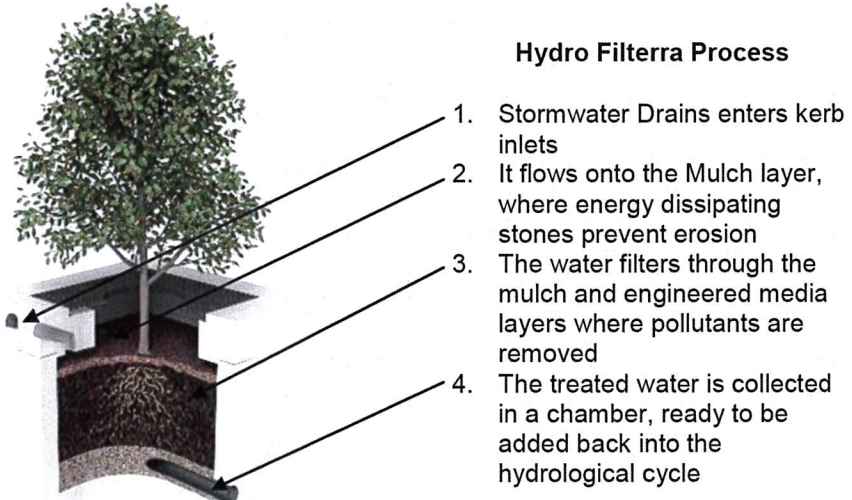


Figure 1 (Hydro, 2011) Diagram representing *Filterra™* process

1.2. An Introduction to Porous Media

The fundamentals of flow through porous media form the basis of governing principles within a broad range of scientific and engineering problems. Applications include areas such as water purification, agricultural engineering, soil mechanics, petroleum engineering, industrial filtration, chemical engineering, environmental sciences, and medical/biological fields. Whilst there may be a wide array of applications of porous media due to the many divisions of engineering and science in which it appears, there seems to have been very little classification of both the structure, and localised behaviour of porous media. The area remains a subject of extensive research and in recent decades, technological developments have allowed a much better understanding of the internal structure of porous materials and their associated flow parameters (Peyton, 1992).

As Bear (1972) points out in his early book on the subject, the term 'porous media' could be defined simply to mean "a solid with holes". However, as observed by the author, this definition is broad and whilst true to an extent, does not allow us to describe or define a porous medium model. Equally, Schriddeger (1958) states "one may be tempted to define 'porous media' as solid bodies that contain pores", but later reveals that this is in no way sufficient. In both cases, the authors suggest that a refined definition is required. The source of discussion lies in the very nature of what is considered to be a "pore". It is simple to assume that 'pores' are the void spaces within the media that do not form part of the solid matrix. Depending on the scale and application considered, these 'pores' could be anything from cavernous openings right down to microscopic spaces between fine grains. Since the point of focus in the case of this paper surrounds the fluid flow within porous media, it seems logical that focus remains on the presence of a 'porous network' or a distribution of voids

throughout the media. With this approach in mind, Bear, Zaslavsky and Irmay (1968) state “we...improve our definition by stipulating that the pores are interconnected, with at least several continuous paths from one side of the medium to the other”. Similarly, Schriddeger (1958) indicates that “a porous system may be interconnected or non-connected. Flow of interstitial fluid is possible only if at least part of the pore space is interconnected”. Using these two descriptions, it is possible to suggest a definition of the fundamental characteristics of what makes up a ‘porous media’. In the case of this investigation, materials that contain interconnected pores, with fluid carrying capabilities are of interest. Many bioretention systems use naturally occurring soil types as porous filter media. This is a readily available material that has high porosity and excellent fluid transport properties, and thanks to organic properties can assist with both inert and active filtration.

1.3. FilterraTM Filter Media

The *Hydro FilterraTM* system utilises a specifically designed organic mix to deliver consistent, regulated filter properties across all systems, giving a high level of both performance and consistency. This mix is made up to a given specification, originally devised by *Americast Inc* and later *Filterra Ltd.* in the USA. However, for application in the UK market, the filter media is currently prepared in the UK by *Hydro Int. (UK) Ltd*, presenting the challenge of creating a mix that matches specification but originates from different soil. Two subsequent considerations are to ensure that filter media created from UK sourced soils meets the US specification, and also to ensure that once in use within the system, the filter media mix continues to display filtration and absorption properties necessary for continued performance. Both of these aspects will be investigated during this project¹.

1.4. Case Study

As part of this group investigation, a case study was carried out, working alongside *Hydro Int. (UK)* on an urban project that features a number of *FilterraTM* bioretention units. The site under investigation is located in Barry, South Wales within a newly developed industrial estate. Other group members conducted work surrounding the implementation of the bioretention unit in an urban environment; however this individual project focuses on the specially engineered filter media within the units under investigation. At the time of a site visit, sampling, and subsequent testing, the case study unit had been in operation for over a year. As such, this formed an important part of the project, as it provided an opportunity to examine the filter media in an active state.

The filter media forms part of an overall composite filtering system that comprises three key phases;

Mulch Layer

This relatively thin top layer is intended to offer an initial, coarse filtering of stormwater, absorbing any macro-scale pollutants such as small refuse, leaves, and suspended large solids. The mulch is combined with energy dissipating stones which prevent high initial flows from damaging the filter media below. “The mulch is an integral component of the system and comprises the surface component for pre-treatment of stormwater runoff. It also serves to protect the media surface and for moisture and weed control” (*Hydro International*, 2011).

¹ The samples of filter media used during this investigation were representative of the mixes used by *Hydro Int. (UK)* at the time of sample acquisition, however consequent testing by *Hydro Int. (UK)* have suggested that modifications have subsequently been made to the ‘UK Media Mix’ used in this investigation. Further explanation of these modifications will be commented on in latter parts of the report.

Filter Media Layer

This layer accounts for the majority of the filter system both in terms of size and filtration capacity. This layer contains the bulk of the root structure from the vegetation, key in the biological processes of the system. Flow through this layer is governed by the laws of fluid flow in porous media. As the purpose-designed, primary filter mechanism, this component shall be the primary area of investigation in this paper.

Gravel Base Layer

The gravel base layer provides a permeable, but stable base for the filter media. It aids in the control of flow through the system but also ensures the filter media is not washed away with the outlet water.

Each of these layers plays an important role within the system as a whole. As a system comprised of mechanical and biological elements, the composite filter design is important in ensuring the system remains functional, with minimal maintenance input required. As the primary filter mechanism, it is thoroughly important that the behaviour and physical characteristics of the engineered filter mix are understood. Focus and detailed investigation in this project will surround the filter media.

2. Soil Structure

The structure, physical characteristics, and internal architectures of soil and its porous system are very important in understanding hydraulic, mechanical and biological processes within a soil matrix. As (Dullien, 1979) states, “practically all macroscopic properties of porous media are influenced to a greater or lesser degree, by the pore structure”.

2.1. Porosity

The porosity, alternatively referred to as voidage, of a material represents the ratio of the pore (void) volume to the total (bulk) volume of the sample. The porosity is a dimensionless quantity, and can be represented as a percentage or as a decimal fraction. If the volume of a sample is assumed to be composed of three phases; solid, liquid and gas, the pore volume can be said to equal the sum of the volumes of the gaseous and liquid phases.

$$\text{Porosity}_{\text{Total}} (\varepsilon_T) = \frac{\text{Void Volume}}{\text{Total Volume}} = \frac{\text{Volume of Gas} + \text{Volume of Liquids}}{\text{Total Volume}}$$

For soils, values for total porosity typically range between 0.25 – 0.7 (25-70%) (Budhu, 2007). Usually, fine grain soils such as clay and silts have a higher porosity than coarse grained soil types such as sand and gravel (Argonne national Laboratory, n.d.). Further explanation of grain size distribution can be found later in this paper.

Whilst total porosity describes the volume of the pore spaces in the sample, it is important to differentiate between types of void space. These can be divided into three clear categories;

Effective Pores

Pore space that is interconnected, forming a continuous phase through the media. Pores that act as a mechanism for transport and fluid flow.

Dead-end/Blind Pores

This pore space is interconnected on only one side. Even though these can often be penetrated, they usually contribute only negligibly to transport and fluid flow. (Bear, 1972)

Occluded/Non-Interconnected Pores

These pores, dispersed throughout the media, are isolated, and not connected to other porous space. Non-interconnected pores cannot contribute to fluid flow.

Due to the presence of occluded/non-interconnected pores, there is the need to distinguish between porosity (as a total value), and ‘effective porosity’. Effective Porosity(ε_E), in this case, is defined as the ratio of the pore volume that can contribute to fluid flow to the total (bulk) volume of the sample. The volume through which fluid flow can occur is smaller than the total volume occupied by voids, and as such, the effective porosity will at all times be lower than the total porosity. Investigation and determination of these parameters is further explored in the experimental section of this project.

An important influencing factor on the porosity of the soil is the size of the soil particles within the medium, described by the particle size distribution.

2.2. Particle Size Distribution

The particles in soil are seldom dimensionally homogenous, and most often have varying shapes. It is for this reason that soil pore geometries are complex and remain an area of continued investigation. The most common way of categorising soil particles is through a Particle Size Distribution (PSD) of the sample. The PSD of a soil represents the range of grain sizes present and the relative amounts of the different sizes. Displayed as a profile, or curve, it can be used to classify soil types and is typically found using the experimental method of sieve analysis (explained further in 5.4). From PSD data the average particle size of the porous medium can be estimated. This parameter is of importance to flow through porous media, as the particle sizes determine the packing and pore architecture of the soil, which in turn affects porosity and fluid transport behaviour. Another important parameter arising from PSD is the effective grain size D_{10} , representing the maximum grain size of the smallest 10% (by mass) of the sample. These small particles effect fluid flow, and through empirical relationships such as Hazen’s Law (2.3.3), allow direct estimation of hydraulic conductivity.

2.3. Permeability/Hydraulic Conductivity

Permeability can be described as a measure of the ability of a porous media to allow fluid to pass through it. It is the term used to describe the conductivity of a porous medium. This hydraulic conductivity is a parameter that arises from the pore space geometry of the media and also the nature of the permeating fluid flow within it. Throughout the early 19th century, a number of key figures produced progressing equations and parameters to describe flow in three dimensions in both steady and unsteady states. Important works arose from Daniel Bernoulli, Claude-Louis Navier, and Pierre Laplace amongst others, many of whose equations still remain at the heart of fluid flow theory. This project will concentrate on two comparable equations related to fluid flow and subsequent hydraulic conductivity of porous media. The ‘Navier-Stokes equation’ and ‘Darcy’s Law’. Experimental and computational procedures allow fluid flow to be approached from these two different angles, with Navier-Stokes providing governing equations of flow applied on a micro-scale to the actual pore geometries of the sample obtained in this project through micro-CT imaging (3.1.2), and Darcy’s Law providing a phenomenological approach from experimentation to estimate flow parameters from a macro-scale (Narsilio, et al., 2009). The methods of experimentation used to compare these approaches are explained further in section (5).

2.3.1. Darcy's Law

It was in 1856 that the first popular theory surrounding the flow of fluids in porous media arose through the findings of Henry Darcy. Having undertaken the project of designing a new water system within Dijon, he published his findings surrounding the flow through sand beds, introducing a macro-scale phenomenological equation applicable to porous flow (Brown, 2003).

Darcy devised a linear law describing laminar flow through homogeneous porous media. He investigated the flow of water through sand filters using the experimental setup shown in Figure 2 below (simplified representation)

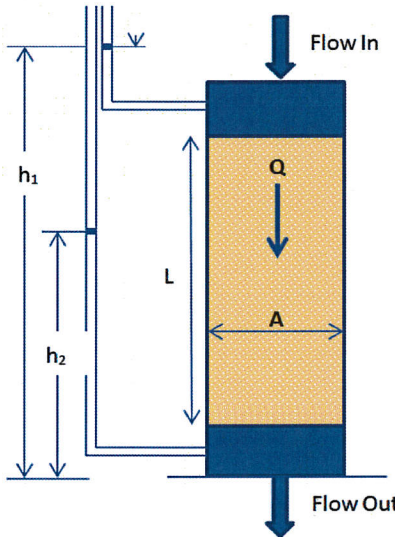


Figure 2 – Darcy's experimental investigation of permeability

Darcy's conclusions show that the flow rate, or rate of seepage, (Q) through the porous media sample (measured as a volume per unit time) is proportional to the cross sectional area of the sample (A), proportional to the difference in total head/pressure drop over the sample length (h_2-h_1), and inversely proportional to the length of the sample (L). This can be described by the equation;

$$Q = -kA \frac{(h_2-h_1)}{L} \quad \text{Equation 1}$$

Or more conventionally;

$$v = -k \cdot i \quad \text{Equation 2}$$

k – Hydraulic Conductivity of the system²

Where,

$$i = \frac{(h_2 - h_1)}{L}$$

i – Hydraulic Gradient, the pressure drop per length

² This hydraulic conductivity k is representative of the 'system', rather than the 'porous media' as it is calculated based on factors arising from both porous media and permeating fluid properties. As (Bear, 1972) notes, "it is a scalar that expresses the ease with which a fluid is transported through a porous matrix. It is therefore, a coefficient that depends on both matrix and fluid properties."

$$v = \frac{Q}{A}$$

v – Effective/Darcy velocity

The effective flow velocity obtained from this equation is representative of the superficial velocity (termed v_s). Whilst useful as a macro-scale value, is not indicative of the local interstitial velocities within the porous network, which will vary throughout the sample and for the most part will be much higher than the superficial value (the cross sectional areas of the pores are far smaller than the area of the tube). Investigation into the localised velocity will be conducted by A.Begley, using models based on geometries provided by the experimental work of this project (5.2).

For an isotropic porous medium, $v = -k \cdot i$ Equation 2 can be written in the generalised form;

$$\mathbf{V} = -k \cdot \nabla h \quad \text{Equation 3}$$

\mathbf{V} is a velocity vector (v_x, v_y and v_z components) corresponding to a point with co-ordinates in a Cartesian system. ∇h is the hydraulic gradient (change in total head), also with components in the x, y and z direction. Substituting the hydraulic gradient for the expression for change in total head, we obtain;

$$\mathbf{V} = -k \cdot \left(\frac{\nabla v^2}{2g} + \frac{\nabla p}{\gamma} + \nabla z \right)$$

(Bear, 1972) and (Narsilio, et al., 2009) state that thanks to low velocities within porous media, the change in piezometric head is much larger than the fraction of kinetic energy, allowing the $\frac{\nabla v^2}{2g}$ term to be ignored, leaving;

$$\mathbf{V} = -k \cdot \left(\frac{\nabla p}{\gamma} + \nabla z \right) = -\frac{k}{\rho g} \cdot (\nabla p + \rho g \nabla z)$$

$$\mathbf{V} = -\frac{K}{\eta} \cdot (\nabla p + \rho g \nabla z) \quad \text{Equation 4}$$

z – vertical co – ordinate

ρ – Fluid Density

η – Fluid Dynamic Viscosity

K – Intrinsic permeability

The intrinsic permeability K can be linked to the hydraulic conductivity k by;

$$K = k \cdot \frac{\eta}{\rho g}$$

2.3.2. Navier-Stokes

The Navier-Stokes equation is a fundamental law of fluid dynamics. It describes flow of viscous, Newtonian fluids with nearly constant density by assuming within a continuum model that the fluid stress is a product of a velocity related viscous term and a pressure term. Under the continuous matter theory from which the equation is derived, it is necessary to define a number of boundary conditions, and as such fluids are assumed to be both incompressible and viscous.

In this investigation, the Navier-Stokes equation is solved within Computational Fluid Dynamics (CFD) models based on actual pore geometries found from micro-CT imaging of the filter media to show the flow at a pore-scale (3.1.2). Equation 4 (shown above) has been derived from the macro-scale experimental expression, Equation 1. However, by following the derivation introduced by (Bear, 1972) and further explained by (Narsilio, et al., 2009), it can be shown that this same expression for Darcy's Law can be derived from the up-scaling of the Navier-Stokes equation that governs flow within pore geometries.

The Navier-Stokes equation, in the form for analysis of pore-scale flow can be shown to be;

$$\rho \frac{\partial \mathbf{v}}{\partial t} + \rho (\mathbf{V} \cdot \nabla) \mathbf{V} + \nabla p - \eta \nabla^2 \mathbf{V} = \mathbf{F} \quad \text{Equation 5}$$

Navier-Stokes, in alternate form from above, for fluid flow in the s-direction at a point inside a pore;

$$\rho \frac{\partial v_s}{\partial t} + \rho (\mathbf{V} \cdot \nabla) v_s + \frac{\partial p}{\partial s} - R_s = -\rho g \frac{\partial z}{\partial s}$$

The right hand side of the equation is a gravity body force, with acceleration due to gravity \mathbf{g} and the vertical co-ordinate, z . The R_s term is a resistive force arising from boundary drag forces of the fluid on the stationary particles, it is assumed to be proportional to mass-average velocity, and acts in the opposite direction to the velocity vector \mathbf{V} . As a local vector force it can written as;

$$\mathbf{R} = -\frac{\eta}{C} \mathbf{V}$$

Where C is a conductance function of the cross-section of the pore. By assuming the resistive force R_s is far larger than the convective acceleration $(\mathbf{V} \cdot \nabla v_s)$, and substituting we obtain;

$$\rho \frac{\partial v_s}{\partial t} + \frac{\eta}{C} v_s = -\rho g \frac{\partial z}{\partial s} - \frac{\partial p}{\partial s}$$

This expression can be multiplied through by $C \frac{\partial \sigma}{\partial s}$, where σ is the local co-ordinate of a streamline such that $v_s \approx v / \frac{\partial \sigma}{\partial s}$. Giving;

$$C \rho \frac{\partial v}{\partial t} + \eta v = -C \left(\frac{\partial p}{\partial s} + \rho g \frac{\partial z}{\partial s} \right) \frac{\partial \sigma}{\partial s}$$

Through volume averaging and transformation back into the x,y,z directions, a governing equation for laminar flow is given. In volume averaging, the porosity term ϵ is introduced, and average variable are indicated with a bar above the symbol;

$$\bar{v}_i + \bar{C} \frac{\rho}{\eta} \frac{\partial \bar{v}_i}{\partial t} = -\frac{K_{ij}}{\epsilon \eta} \left(\frac{\partial \bar{p}}{\partial x_j} + \rho g \frac{\partial z}{\partial x_j} \right)$$

K_{ij} is the permeability tensor, a function of the average conductance of the pores. The second term $\bar{C} \frac{\rho}{\eta} \frac{\partial \bar{v}_i}{\partial t}$ is assumed to be negligible as it represents local accelerations that can be ignored for the low Reynolds numbers typical within porous media.

Multiplying the expression by the porosity (ϵ) allows the effective velocity to be found. This expression represent the same effective velocity that is shown in Equation 4 but derived from the up-scaling of the theoretical incompressible Navier-Stokes equation, rather than the experimental derivation previously explained (Bear, 1972) (Narsilio, et al., 2009).

Darcy's Law from Upscaling of Navier-Stokes $v = -\frac{K_{ij}}{\eta} \cdot \left(\frac{\partial \bar{p}}{\partial x_j} + \rho g \frac{\partial z}{\partial x_j} \right)$ **Equation 4**

Darcy's Law from Experimental derivation $V = -\frac{K}{\eta} \cdot (\nabla p + \rho g \nabla z)$ **Equation 6**

The derivation outlined above shows compatibility between the two derivations of this law. It is shown theoretically, that thanks to governing equations, a direct comparison can be made between the hydraulic conductivity calculated using micro-scale³ models created from pore-scale geometries and the hydraulic conductivity calculated from macro-scale experimental testing.

2.3.3. Hazen's Law

Empirical relationships exist to relate the permeability and hydraulic conductivity of a porous media directly to experimentally-determined physical properties. This project uses imaging techniques to assess hydraulic conductivity based on micro-scale geometries. However, as a method of further comparison, the empirical relationship outlined by Hazen (1930) shall be considered to estimate hydraulic conductivity from geotechnical testing. Hazen (1930) states;

$$K = C_1 (D_{10})^2 \quad \text{Equation 7}$$

Where C_1 is a constant of range 0.4-1.5 dependent on soil type, and D_{10} is the effective size (further explained in section 6.3).

2.3.4. Packed Bed Theory

A large part of the computational and theoretical work to be carried out by other group members involves the investigation of the relationship between flow velocities and pressure drops within the filter media. This work is based on an assumption that flow through the filter media is analogous to flow through packed beds, where the filter media can be described as number of spheres representing the average particle size present. As such, the equations and relationships used derive from the Navier-Stokes law outlined above, but incorporate parameters and theory associated with packed beds. As part of the experimental stage of this project, investigation will be made as to the validity of this assumption of analogous behaviour (5.6).

Theoretical discussion of flow through packed beds is presented in detail in the works of (Begley, 2012) (Pavey, 2012). There are a number of empirical correlations used to calculate pressure drops within a packed bed, including those of Ergun, Carman-Kozeny and Blake, explained by (Begley, 2012) (Pavey, 2012). The theory of these correlations does not form part of this individual project; however it is important to identify some key terms that shall be used at a later point for comparison between experimental results and CFD, along with investigation into the validity of packed bed theory applied to flow through granular soils. For full explanation of terms, see (Begley, 2012) (Pavey, 2012) (Baker & Tabor, 2010).

³To call the Navier-Stokes a method of micro-scale investigation is purely a relative term in the case of this report, where this approach will be directly compared to Darcy's experimental (macro-scale) analysis. A more appropriate term may be 'pore-scale', as Navier-Stokes arises from continuum matter theory, where the fluid is considered as a continuous medium (Scheidegger, 1960), which neglects molecular structure of the fluid, however in this case we will refer to this 'pore-scale' based approach as the 'micro-scale' aspect.

R_e , the Particle Reynolds number

This dimensionless parameter allows a comparison of flow conditions between models and experiments of differing porous media and fluid properties, important in allowing the validation of CFD models using experimental procedures. It can be described by the equation;

$$Re_{dp} = \frac{\rho U d_p}{\mu} \quad \text{Equation 8}$$

Where, ρ is the fluid density, d_p is the average particle size (see 5.4), U is the superficial velocity, and μ , (as before) is the kinematic viscosity of the permeating fluid (Bear, 1972) (Dullien, 1979). (Begley, 2012) and (Pavey, 2012) further define flow regimes for a range of the particle Reynolds number, where the flow can be characterised as laminar ($Re_{dp} < 10$), transitional ($10 < Re_{dp} < 300$) or turbulent ($Re_{dp} > 300$), based on works of (Baker & Tabor, 2010).

ϕ , Dimensionless Pressure Drop

For direct comparison; experimental, theoretical, and computational results can be reported in the form of dimensionless pressure drop, where;

$$\phi = \frac{\Delta P \cdot d_p}{\rho U^2 L} \quad \text{Equation 9}$$

The packed bed theory is applicable to air flow tests conducted on samples of the filter media, further explained in (5.6). The geometries used for these models, and the CFD models to which they shall be compared are obtained through the imaging of the filter media.

3. Imaging Techniques

Until recently, there was little known about the complex nature of the internal structure of soil. There have been investigations and a plethora of methods adapted in an attempt to define porous systems. The main obstacle to this understanding lies in the opaque nature of the material. Characterisation of the 3D network of pores within soil was previously restricted by the absence of precise, easy to use, reliable methods for geometrical investigation (Anderson, et al., 1990). There are two main characteristics of early imaging methods. The first is that they typically gave a 2D representation of pore structure, with spatial discontinuity and limited understanding of whether pore channels were connected. Secondly, they were destructive; in that samples would have to be changed in some way prior to, or during, testing. The problem of discontinuity acts in limiting accurate representation of fluid flow, as it is only the interconnected porous ‘channels’ that allow flow. ‘Dead-end pores’ that do not aid fluid transport should be identified within samples. As (Heijmans, et al., 1995) state “There is a need for non-destructive techniques for the quantification of soil structure that enables the investigation of undisturbed soil material without any further preparation and/or drying”. New developments in imaging of materials have provided tools to overcome this challenge, offering non-destructive methods with wide applications. “Conventionally....the soil pore system is inferred from the flow dynamics using relationships between pore diameters and the measured volumes of fluids. Image analysis of soil porosity provides a means characterising the actual, rather than the inferred morphology of soil pores.” (Grevers, et al., 1989)

3D imagery of earth and organic materials is a new and developing area within geosciences. As (Carlson, 2006) observes, “Technologies that generate three-dimensional imagery of geological materials are now stimulating new discovery and answering old questions”. The

three most applicable techniques used in geosciences are X-Ray Computed Tomography (XCT), Magnetic Resonance Imaging (MRI) and Neutron Computed Tomography (NCT).

3.1. X-Ray Computed Tomography (XCT)

In 1971, the first commercial Computed Tomography Scanner, designed for use in brain scanning was built by Cormack and Hounsfield. As designs evolved, through the 1980's CT scanning became a popular and widely used technology, with a wide range of medical applications (Robb, 1982). The Earliest records of effective use within the soil sciences appear from (Petrovic, et al., 1982). The early applications of XCT in modelling soil were important in beginning a new approach to soil understanding. These approaches also highlighted some adaptations to the XCT procedure used in the medical field that would enhance results for the new-found solicitation.

3.1.1. Principles

XCT systems are designed to illuminate an object with X-Rays travelling along multiple paths and to measure the reduction in beam intensity along each of those paths (Carlson, 2006). The sample or object to be scanned is located between an X-Ray source and an X-Ray detector. The attenuation of each ray is measured as it passes through the sample, usually by a conical configuration of X-rays beams and arc of detectors, although different configurations are available (cone-beam, fan beam, or parallel beam). Utilising a rotational motion of the sample relative to the source-detector system, a view of the sample is possible from multiple angles (Cnudde, et al., 2006). The rotations are systematic, and give a number of 2D radiographs of the sample at different rotation angles between 0 and 360°. As the X-ray beams pass through the sample, they are affected by the density and atomic number of the material through which they pass (Cnudde, et al., 2006). Attenuation of the X-Ray beam is dependent on photon energy absorption within the absorbing medium, caused by the creation of photo-electrons and Compton Scattering. Photo-electrons are created when the material absorbs X-Ray photons, thus reducing the energy of the beam. This absorption is related to the mean atomic number of the sample medium. Compton scattering is the process whereby the interaction of a photon and electron cause an inelastic scattering of the photon from its original path and a consequent reduction in X-ray energy. An array of detectors measures the degree of this attenuation for each beam, in the form of a linear Attenuation Coefficient (AC) (Heijmans, et al., 1995). The data is converted into digital radiographs, building up a series of AC values for the multitude of rotation angles, with an AC for each pixel/element within the scan field.

AC values vary from scanner to scanner and are expressed relative to datum coefficients using the linear scale of Hounsfield Units, in order to normalise results. Using this linear scale, CT data has reference values, as water has a Hounsfield Unit of 0 and air has a value of -1000, allowing the definition of the HU's for a range of standard materials. These values for standard materials, when applied in conjunction with values for air, allow calibration of equipment.

A collection of scans through the full range of rotation angles are processed using some form of tomographic reconstruction software based on mathematical algorithms. This technique, known as filtered back projection compiles the data from a number of scans to create a 2D representation of the cross section (Narsilio, et al., 2009).

Multiple stacked images and 2D slices, taken at small increments can be combined to give a 3D model. The 2D pixels when converted into 3D elements are referred to as Voxels, the size of which depends not just on the pixel size, but also the increment between scanning planes. The CT image is essentially a map of the AC values (Grevers, et al., 1989). The data in this 3D

model is based on a HU assigned for each voxel through the sample. The Hounsfield values for the different voxels (elements) can be represented on a grey scale, allowing a visual model where the density of different parts is depicted by the intensity of the grey scale (typically denser materials have whiter pixels, visually representing a higher HU value). (Further investigation shown in 5.7)

3.1.2. Micro-CT

XCT scanners are designed to be used on samples of varying size and densities. Larger objects, or objects with a higher density may require a higher energy X-Ray beam, in order to ensure the beam penetrates the sample. In the medical field, densities are typically low, and the spatial resolution required is not microscopic, so large apparatus with lower energy X-Ray beams is used. For the geosciences and engineering applications however, the materials are usually of a higher density, and the spatial resolution is usually required to be far smaller (Carlson, 2006), and as such high energy X-Ray sources and high resolution detector systems are used. These smaller high powered scanners are known as micro-CT scanners. Whereas in the medical field, the X-Ray strength must be limited for health reasons, for materials applications, maximum X-Ray energies can be used, and where samples in the medical field are on a large scale, material samples can be tested on a smaller scale, with higher resolution. The configuration and type of apparatus used is selected dependent on the sample size and spatial resolution required.

The spatial resolution that can be obtained from a XCT scan is dependent on 4 key factors;

Magnification

Defined as the ratio of the source and detector to the source and sample. X-rays are in a conical geometry, so to obtain higher magnifications the sample must be brought closer to the source, whilst ensuring the whole sample is still in the field of view. In medical applications, the patient is usually in the centre of the scanner, giving a magnification factor of 2. There is a trade-off between sample size and magnification; hence smaller samples which can be positioned close to the source allow a greater magnification.

Focal Spot Size

This is reliant on the X-Ray tube type. In micro-CT, a small spot size must be used to yield high spatial resolutions, and this reduced size is made possible by a much lower current.

Pixel Size of Detector

Technological developments have increased the accuracy of detectors. This component is of vast importance, as tomography is improved with higher pixel resolution, and resolution is limited by the detection pixel size.

Physical Phenomena

Relating to unwanted interferences that cause difficulties and inaccuracies in the collected CT data, most importantly X-ray scattering. See (3.1.3)

With most medical scanners, the source-detector configuration rotates around the stationary patient. In the case of small scale applications such as soil investigation on the other hand, it is easier if the sample is rotated, and the source-detector mechanism remains stationary. As (Mees, et al., 2003) states “The advantages of micro-CT systems for material research include the possibility of attaining higher resolutions by using micro-focus X-ray tubes and by rotating the sample rather than the source and detector”.

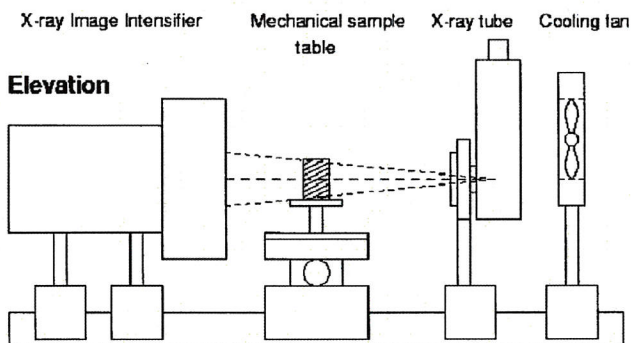


Figure 3 (Gregory, et al., 2003) – Simplified layout of a micro-CT scanner

3.1.3. Considerations

XCT is a very useful and highly advanced technique; however there are a number of factors that can cause complications not only in the collection but also in the interpretation of CT data. These can be overcome through careful consideration and adaptation of apparatus along with post-scan manipulation and rendering. The first complication or consideration that arises regards the internal processes that cause X-ray attenuation.

Attenuation Considerations

The photoelectric absorption (explained previously) is controlled by the mean atomic number of the material and is the dominant process at lower scan energies. The Compton Scattering effect on the other hand is the predominant process at the higher X-ray energy level, and is less dependent on the mean atomic number. The scans at a higher energy show attenuation differences which arise primarily from mass density differences, whilst the lower energy scans are more reflective of the compositional differences in atomic structure. If the material within a sample varies primarily in atomic structure, then the low-energy X-ray may present a problem with penetration of the sample. It is due to this difference in representation that the X-ray energy levels for scans must be adapted to the material and type of scan required.

Scanning Artefacts

Scanning artefacts are discrepancies between the CT numbers in the reconstruction and the actual AC values for the sample. Some artefacts can be reduced by modifications of the conditions prior to image acquisition, other require modification in the latter reconstruction phase (Mees, et al., 2003). The primary artefacts within XCT that should be considered are;

- **Misalignment Artefacts**
 - Throughout the full 360° rotational scan, there may be small errors in axial alignment between the source, sample and detector. These can be overcome by ensuring that the rotational equipment maintains a steady and accurate axial alignment throughout rotation.
- **Ring Artefacts**
 - Detector variations such as this are typically caused by mis-calibration, and with careful calibration and field of view optimisation these artefacts can be minimised or removed completely. (Barrett & Keat, 2004)
- **Star Artefacts**
 - The presence of objects with a much higher density than the rest of the scan medium can cause star artefacts. These are usually caused by anomalies within the medium and can usually be removed during the latter reconstruction phase.

- Beam Hardening

- This is the most influential artefact within XCT scans. Beam hardening appears in XCT imagery as an artificial reduction of attenuation near the centres of long X-Ray paths (Carlson, 2006). This artefact can be reduced or removed by hardening the beam prior to contact with the sample, using a filter. Another method is scanner calibration, whereby compensation in beam intensities is applied to the source. Ensuring a calibration of X-Ray energy relative to sample size can reduce the beam hardening effect.

3.2. Alternative Techniques

Neutron Tomography (NCT)

The technique for NCT is very similar to that of XCT. A neutron beam is passed from a neutron source, through the sample, and the attenuation is measured using a sensor method. The primary difference between XCT and NCT lies in the interaction of the beam with the specimen. As (Winkler, et al., 2002) explain, “The transmission of a sample depends on the neutron-absorption and scattering cross-sections and the concentration of the isotopes present in the sample.” The most effective attenuation of neutrons arises from Hydrogen, and as a result, contrast within NCT images is dominantly determined by Hydrogen content. Hydrogen causes an almost negligible X-ray attenuation (Carlson, 2006), so NCT images can show different aspects of a sample, often useful when considered alongside XCT scans.

Current NCT methods are limited in the resolution and spatial resolution that they can achieve. The spatial resolutions are much lower when compared to XCT methods, due to a greater number of scanning artefacts and the large scattering effect associated with the neutron imaging (Masschaele, et al., 2001). NCT highlights elemental differences within a sample through the interaction with atomic nuclei, and can give useful results that represent alternate characteristics to the XCT technique. In this investigation, the focus is on the porous network, rather than the element differences of the material, and as such, this method is not preferred to XCT. In addition, limitations in current apparatus technology and availability make the NCT approach unsuitable for the work carried out in this project. Using NCT scanning alongside XCT would be an area of further development and interesting area of research for the future.

Magnetic Resonance Imaging (MRI)

Unlike XCT and NCT, in MRI, incident beams are not passed through the sample, instead a magnetic field is progressively applied in pulses and at different gradients. The magnetic resonance of the scan is influenced by the position of the nuclei within the sample elements. The limitation when applied to soil samples lies in the fact that the technique relies on elements with unpaired nuclear spins. In medical applications, there is a greater abundance of these elements, the most common of which is ¹H, but as (Carlson, 2006) states “..Hydrogen in rigid solid phases does not yield a detectable signal in standard MRI, so the technique is strongly focused on fluids.” This approach is more suited to fluids than a solid matrix such as soil.

3.3. Micro C-T Application

The technique of micro-CT has clear advantageous application to the study of the internal porous structure within soils and other porous materials. Whilst other techniques offer potential within the geoscience field, micro-CT technologies that are currently commercially available seem to offer the most accurate, yet simple method of 3D modelling.

The results of micro-CT imaging are used in four different ways within this group project;

1. Creation of micro-scale and macro-scale CFD models of the different samples of filter media based on the geometries obtained.
2. Volume rendering of the scan data to create 3D visualisations of the different filter media.
3. Creation of Additive Layer Manufactured (ALM) model of a section of the filter medium, with the same geometries as the CFD model, for use in experimental flow tests to validate CFD results.
4. Investigate AC outputs in graphical form to look into ways in which different parts of the filter media can be identified and categorised from micro-CT⁴.

This work covers a vast array of technical areas, requiring a large amount of experimental work and computational modelling, as such, the work undertaken in this individual project was undertaken alongside work by other group members, with a constant flow of information and data between parties.

4. Experimental Project Management

4.1. Group Management

After discussion and an assessment of individual skills, the group was divided into two smaller sub-groups, one concentrating on experimental work and the other on computational work (CFD). The focuses in each of these sub-groups are bespoke to the problems at hand, however communication and on-going exchange of resources ensure the overall group progress remains consistent. Regular meetings and discussions allowed a continual, two-directional flow of information between the groups. As the responsibility for the micro-CT scanning of the samples was part of this individual project, the importance of accurate, representative, and useful results was fundamental. The individual experimental tasks undertaken by the author contribute towards all five of the points stated above, and can be summarised into the phases shown below. Although these phases reflect sub-divisions of the individual work to be carried out, it is important that they are considered as part of a larger, group project. Figure 4 shows a flow chart of the various experimental aspects of the project, and how the work conducted by the author contributes towards the group framework.

4.2. Individual Management

During the initial planning phase of the project, a number of clear experimental phases were identified to form the content of the individual project undertaken. Added importance of phase-planning arose due to a need to address the issue of availability and scheduling of resources and equipment. The equipment being used is in high demand, and work scheduling must take into account availability of resources and of the professional operatives required for processes such as scanning and rapid prototyping (shown in Gantt Chart in (Please, 2011)). The phases can be divided into the following groups.

⁴ This part of the project arose from extensive investigation into micro-CT technology, and whilst not of direct application to fluid flow properties, is an important finding of this individual project and an area with potential for further progress.

Phase 1: Research of X-Ray CT and micro-CT methods

1.1 - Research into the topic to gain a detailed understanding of the principals and technology surrounding the technique(s). Research in to scanning considerations. This phase utilises journal articles, books and other resources. The findings are presented in the report “I1” (Please, 2011) and summarised during the first part of this report.

Phase 2: Scanning Initial stages and Experimental Protocol Design

2.1 - Modification of experimental technique. As Micro-CT apparatus and technique must be modified to suit the sample type and testing conditions, this is an important phase, giving rise to a finalised testing technique and protocol.

2.2 - Scanning of initial samples. Scans of a number of initial samples conducted, firstly in order to modify and calibrate the scanning protocol, but also to supply data for other group members. Those group members working on CFD modelling will use the data from these initial scans in order to produce initial meshes and models.

Phase 3: Scanning of filter medium sample extracted from macro-scale permeameter test

3.1 - Other members of the group shall be performing macro-scale flow experiments on the filter media using permeameter apparatus and the application of Darcy’s Law. Core samples should be extracted from these tests and scans carried out to determine the topography of active samples.

Phase 4: Scanning of filter medium sample extracted from case study system

4.1 - As part of the group project, there shall be a site visit and case study conducted. A core sample from this active bioretention system will be extracted and scans carried out to determine the topography of a real-life sample. The results of both Phase 3 and Phase 4 will be passed to the CFD team to create models.

Phase 5: Sieve Testing and PSD investigation of the various filter medium samples

5.1 – Sieve testing conducted to investigate soil characteristics of the different samples, both for comparison, and to obtain average particle diameters for use in models.

Phase 6: 3D Model construction and Rapid Prototype of scanned profile

6.1 – A 3D model of a section of the sample from phase 4 will be produced. A rapid prototype of this region will be created using laser-sintering technology. This model will be an enlargement of the scan profile, used to visually display the porous zones in a magnified manner, and will be tested in a purpose-built, sealed apparatus using air flow.

Phase 7: Flow tests on Rapid Prototype sample

7.1 – Rapid Prototyped model is tested in a sealed apparatus and subjected to various different flow rates.

7.2 – Using the pressure drop measured across the sample and the application of Darcy’s law, the experimentally derived permeability can be calculated. The results from this experimental investigation will be used as validation of the CFD models.

Phase 8: Comparison of results

8.1 – Permeability/Hydraulic Conductivity from Phase 6 will be compared to the figures obtained from the CFD models produced from the same scan data, and the macro-scale permeameter tests.

Phase 9: Attenuation investigation

9.1 – As an extension to the project, investigation into the AC distribution within the samples will be conducted, with comparisons made between different samples and exploration into further applications of the technology/methodology.

These nine phases indicate the clear steps that will be carried out to produce an overall investigation into the fluid flow behaviour within porous media. The flow chart below shows a simple representation of the experimental processes and the links and dependencies within the project.

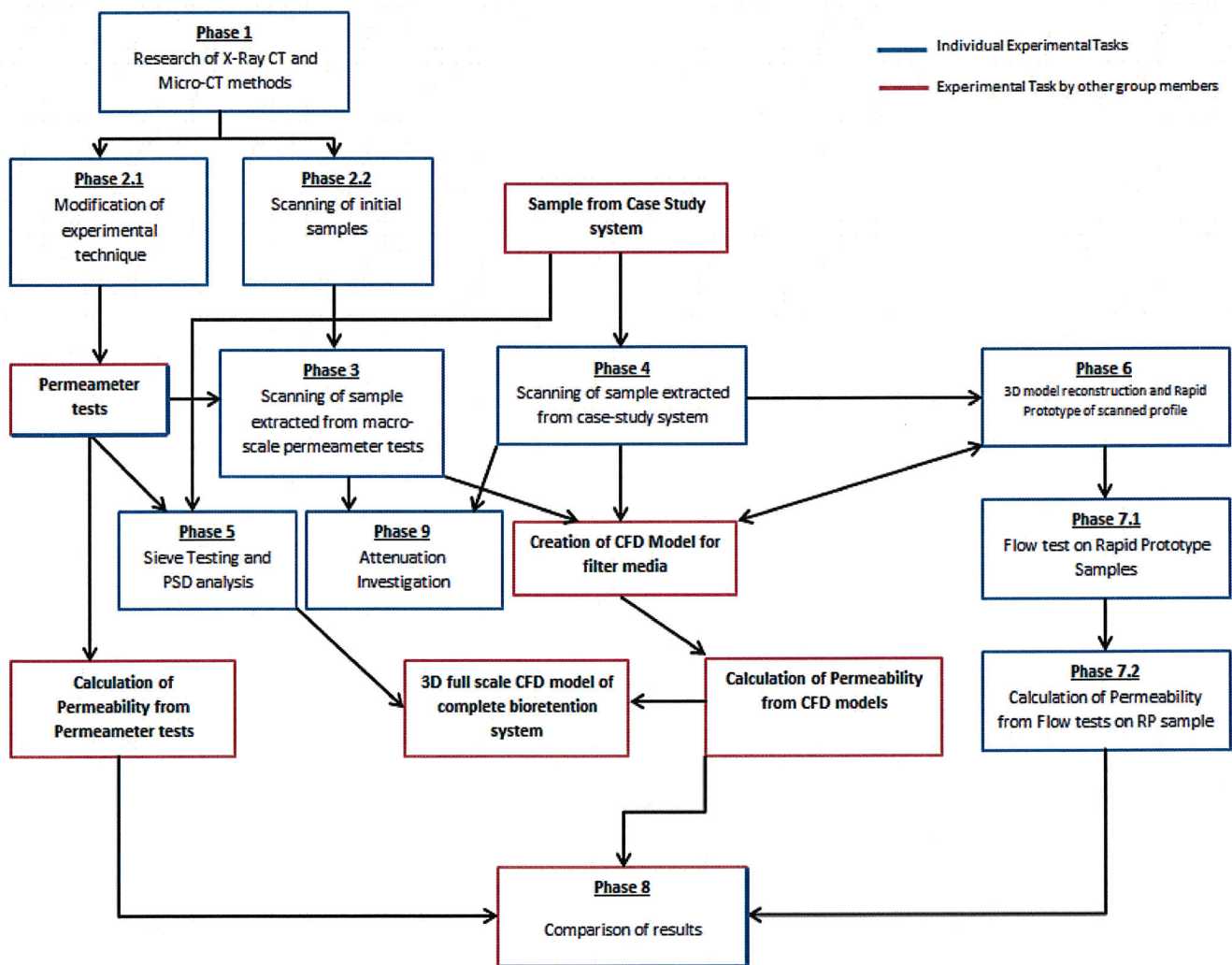


Figure 4 - Flow of Experimental Project Management

5. Methodology

5.1. Phase 2: Scanning Initial stages and Experimental Protocol Design

The equipment used for the micro-CT scanning is a state of the art *X-Tek Benchtop CT* machine at the University of Exeter. The scanner consists of a high contrast image intensifier and 60W, 5 micron x-ray source, which can operate in the 25 to 160kV range of peak energies. Through the use of metal filters, the X-ray beam energy can be adjusted to suit application. The object to be scanned is positioned on a precision, 5 axis, manually controlled manipulator, between the source and detector array. Angular projections are acquired through object rotation by the manipulator. For each of the experiments 2500 angular projections were acquired for every scan. With a maximum scan area of 200x200mm, the system is able to achieve geometric magnification of 100x and voxel sizes down to 5 microns. The user interface and control console allow full control of the scan settings. The dual function of the system allows the samples to be interrogated at a low resolution with very short scan times, and in higher definition with a longer, full scan cycle (X-Tek Xray Systems, 2006).

The images below show the (a) user control interface, (b) complete system, and (c) an example of a scan setup;

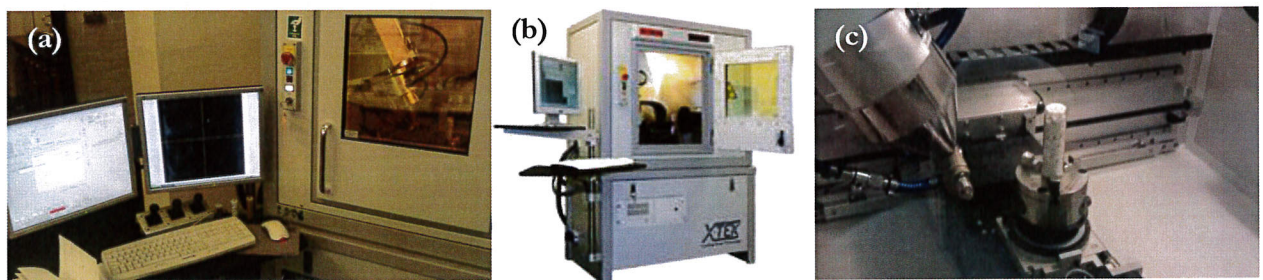


Figure 5 – Images of the 'X-Tek Benchtop CT' micro-CT Machine (X-Tek Xray Systems, 2006)

5.1.1. Phase 2.1 – Modification of Experimental Technique

Sample Capsule

The first stage in sample preparation for scanning was to decide on an appropriate material to use as a sample capsule. The important characteristics of this capsule were that it would not interact in any way with the sample, would not affect x-ray attenuation, and would be of a density such that it allows full penetration of x-ray beams at the stated energy levels. In the past, the apparatus had been used to test a number of organic and non-organic materials, although had not been used on soil samples. The materials tested were PVC tubing, Glass tubing, Perspex tubing, and Card tubing. It was decided after a number of low resolution 'fast' scans that Glass was the most suitable material.

With a decision made to use glass as the sample container material, initial scans of a number of materials can be made to provide intial data. These initial scans were conducted with two aims;

- Providing initial data for the CFD group. This allowed the primary experimentation with mesh creation and CFD modelling prior to implementation with the actual filter media.

- Modification of the scan protocol, in particular sample dimensions and image reconstruction methods.

Cylindrical samples were used as this not only ensured core sampling simplifications, but also aided in the optimisation of scan results and to minimise scan artefacts. During rotation, by ensuring a constant length over which the X-Ray beams must penetrate, the effects of beam hardening and other phenomena remain consistent throughout the imaging process. As (Heijls, et al., 1995) state “artefacts will be minimal when the path lengths of the photons through the material are approximately constant. This can be obtained if one uses cylindrical samples.”

Given that soils and gravels have a relatively high density, as explained in the theoretical part of this paper, there is a need for a high energy level X-Ray source to permit sufficient penetration for accurate attenuation measurements. In the first scanning of the trial samples, sample diameters of 50mm and 25mm were used, to find the optimum diameter for future testing.

Using various scans on a gravel sample (deemed to have the upper limit of density present in the filter media to be tested in future phases), a sample diameter of 25mm was reasoned to be most appropriate. The height of the sample was set at 75mm, as this was the standard tube length easily available. During scanning however, the scanned volume is not the complete sample length. A section of length 30mm is scanned. By imaging only this required portion of the sample height, magnification is increased.

A copper filter was used on the scans. The polychromatic spectrum from X-Ray tubes in micro-CT scanners can cause beam-hardening, due to the preferential attenuation of the lower-energy beams and resultant spectrum shift toward higher-energies. The copper filter applied filters out the lower-energy beams from the applied X-Ray, thus reducing the beam hardening effect (Sensen & Hallgrímsson, 2009). Using a filter to regulate x-ray energy, and operating at an X-Ray level in the range of 130-160kV the scan protocol was deemed to be appropriate to continue to consequent experimental phases.

5.1.2. Phase 2.2 – Initial Scans

Once the experimental procedure had been assigned, and the optimum sample sizes found, full, high resolution scans were carried out on three initial sample materials. The soil types chosen for these initial samples were (i) Coarse Gravel, (ii) Fine Gravel, (iii) Sharp Sand (images of samples in Appendix B)

These three initial sample materials were chosen as they gave a wide range of particle sizes and also a range of densities. In the initial phases of the experimental procedure, it is important to obtain data for a range of conditions in order to consider which methods and applications will be most effective in future phases. The filter media, which is tested in phase 3 and 4 is a well distributed media, with a wide range of particle sizes, as such, the choices of samples in this initial testing phase were designed to ensure a wide scope of application.

An additional reason for the choice of sample materials was due to the requirements of the CFD modelling team within the group project. The software being used to model flow is both complex and new to the individuals involved. By supplying micro-CT data for a range of soil types, and more importantly particle sizes, those individuals were able to build up a number of meshes and models, improving their skills but also increasing the probability of obtaining accurate, useful models during the future phases.

The three samples were modelled separately, although the scanning setup was almost identical for all cases. The X-Ray source was operated at 115kV. A current of 115uA for #1 and #4, and a higher value 140uA for #2 and #3 was applied. A copper filter of thickness 0.25mm was applied to all scans. A long, detailed scan of 2500 projections was taken in each case. The results for these initial scans can be found in section 6.1 of this report.

5.2. Phase 3: Scanning of filter medium sample extracted from macro-scale permeameter test

Upon request from the author, *Hydro Int. (UK) Ltd.* provided a large sample quantity of engineered filter media for use in the investigation. This filter media consisted of specified gradation of washed aggregate and organic material homogenously blended under strict quality controlled conditions, and had been formulated based on design specification. The sample was assigned the label 'Hydro Lab Sample'.

Permeameter Testing

Working alongside a fellow student within the experimental group, a number of permeameter apparatus were designed with the specific goal of testing the hydraulic conductivity of the filter media on a macro-scale. These experimental apparatus were designed to allow investigation of both the filter media individually and the combined system of filter medium, gravel and mulch layer.

3 small, Bench-scale column tests were setup. These setups allowed daily testing of flow rate through the sample volumes. The experimental setup consisted of a column, with a reinforced mesh section at the base, supported on a testing surface. A test volume of water was added to the system from above, and the flow rate measured through collection in a calibrated vessel below the testing surface over a timed period. Tests were repeated on a daily basis over a number of weeks to ensure a steady value of hydraulic conductivity was achieved. This was necessary as the wetting and drying of the media during and after flow tests expands and contracts organic content within the system, which help in the creation of preferential flow pathways (Americast Inc., 2009). The three, bench-scale permeameter setups consisted of;

- Permeameter #1 – 'Hydro Lab Sample' filter media
- Permeameter #2 – Scale model of composite filter volume, with 3 layers in scaled proportions according to specification (Mulch, Hydro Lab Sample, Gravel) (Hydro, 2011).
- Permeameter – Designed to accommodate sample media from case study, sampled for testing at a later date as part of a later experimental phase.

A larger permeameter was also constructed, using a similar design to the smaller permeameters, and modified in order to accommodate a tree within the column test apparatus. This setup was designed with the specific goal of creating a laboratory scale version of the full bioretention system. As with the smaller setups, flow experiments were conducted on a daily basis, with standard falling-head permeameter experimental process followed to investigate hydraulic conductivity of the system as a whole. The design phase of this aspect was undertaken alongside fellow group member L.Whitehurst, however the experimental data collection was performed individually by L.Whitehurst. Images and further details of the different permeameter experiments can be found in 'I2' (Whitehurst, 2012).

Extraction of Sample

Initially, it was decided that the sample of filter media should be core-sampled from the permeameter test #1 (Hydro Lab Sample). However, the permeameter rigs were not setup and functioning at the planned time (shown in Gantt chart in 'I1' (Please, 2011)). Due to time constraints and the need to begin the first scanning process, it was decided that a sample

should be taken directly from the filter media provided, prior to the permeameter testing. This change in experimental scheduling ensured the CFD group were provided with necessary data without a delay. A sample was taken, ensuring that the large quantity supplied in bags was well mixed prior to sampling to give a sample representative of that which would be present in the permeameter tests.

Scanning Process

After a number of test scans at a fast scan time, the sample was scanned using a detailed, 2500 projection, full length scan time. The X-Ray source was operated at 130kV, with a current of 135uA, and a copper filter of thickness 0.5mm applied to the beam.⁵

5.3. Phase 4: Scanning of filter medium sample extracted from case study system

Site Visit

Organised in collaboration with *Hydro Int. (UK)*, the group travelled to Barry in South Wales to meet with representatives from the company at the first installation site of the *FilterraTM* system within the UK. A full site visit was conducted, with inspection and discussion of each unit, concentrating in particular on the technical details surrounding the designs. Full drawings and design specifications were provided.

Extraction of Sample

Samples of the filter media were taken from the unit that had been selected for use in the case study (further details of case study unit outlined in '12' (Winston-Gore, 2012)). The samples were extracted using a small trowel, removing the steel grating above the unit, digging through the mulch layer and into the main filter media layer of the unit and extracting a sample from the top section of the filter media layer. The samples were immediately transported back to University of Exeter for use in experimental testing, with one large sample volume used in the permeameter tests (Permeameter #3 from 5.2 above), and the other samples for use in the micro-CT scanner and sieve testing. The samples were assigned the label 'Case Study Sample' media.

Scanning Process

After a number of test scans at a fast scan time, the sample was scanned using a detailed, 2500 projection, full length scan time. The X-Ray source was operated at 110kV, with a current of 100uA, and a copper filter of thickness 0.25mm applied to the beam⁶.

5.4. Phase 5: Sieve Testing and PSD investigation of the various filter medium samples

Sieve Testing

As the filter media is a coarse-grained soil, the distribution of particle sizes or average grain diameter can be found by sieve testing, involving screening a known weight of soil through a stack of sieves of progressively finer mesh size (Budhu, 2007). Sieve testing was conducted to compare the particle size distributions of the different samples of the filter media, and to obtain an average particle diameter for use in CFD processes and later phases. 3 sieve tests were conducted on Hydro Lab Sample, Case Study Sample and also on a third sample of the *Filterra^{TM USA}* Specification filter media provided by *Hydro Int. (UK)*. British Standard sieve testing procedure was followed, with samples oven dried prior to testing. 7 sieve sizes were

⁵ Scanning process conducted by Dr. Lesley Wears

⁶ Scanning process conducted by Dr. Lesley Wears

used, with the smallest sieve diameter of 300 microns and largest of 5mm. Tests were conducted in the structural engineering laboratories at the University of Exeter using the sieve shaking table apparatus.

5.5. Phase 6: 3D Model construction and Rapid Prototype of scanned profile

3D Model Creation

From 2D scan data obtained in phase 3 and 4, the internal volume of the samples is reconstructed using inverse problem techniques (tomography) (Narsilio, et al., 2009). The different x-ray absorption coefficients are assigned grey-scale values and 2D cross sections of the volume are reconstructed. These 2D images are enhanced and improved using post-scan noise reduction facilities within the X-Tek scanning apparatus. Ring artefact minimisation and shading correction applications are also applied to the 2D images. The software “Ct Pro 3D” was used on a high powered reconstruction computer to convert the 2D images into a 3D volume. The image rendering program “VG Studio Max 2.1” was used for additional volume rendering tasks and image enhancement. Images of the models created can be found in the results section. From the 3D volume-rendered image, a full *dicom* format extract of the pore-scale structure was delivered to the CFD group for Image Based Meshing (IBM).

Additive Layer Manufacturing (ALM)

An ALM model of the 3D filter media geometry was created using the identical CFD model geometry in order to validate CFD results with experimental testing (5.6). For this process the case study sample was selected, as a sample from an active bioretention system would be the most representative of the samples with regards to the micro-architecture and porous network configuration.

A sample of length 12.85mm and diameter 12.73mm was selected to be used in both the CFD model and flow tests and extracted from the central region of the 3D scan model. The reduced diameter volume was used to ensure wall effects from sampling and packing within the tube would not affect results. A 3mm thick skin was applied to the model to ensure it remained structurally intact during manufacturing and later testing. This smaller sample was up-scaled by a factor of 7.778 to give a model of length 100mm and diameter 99mm (these dimensions were selected to correspond with the apparatus used in phase 7). Figure 6 shows the dimensions of the original scan and the up-scaled model of the extracted region for ALM.

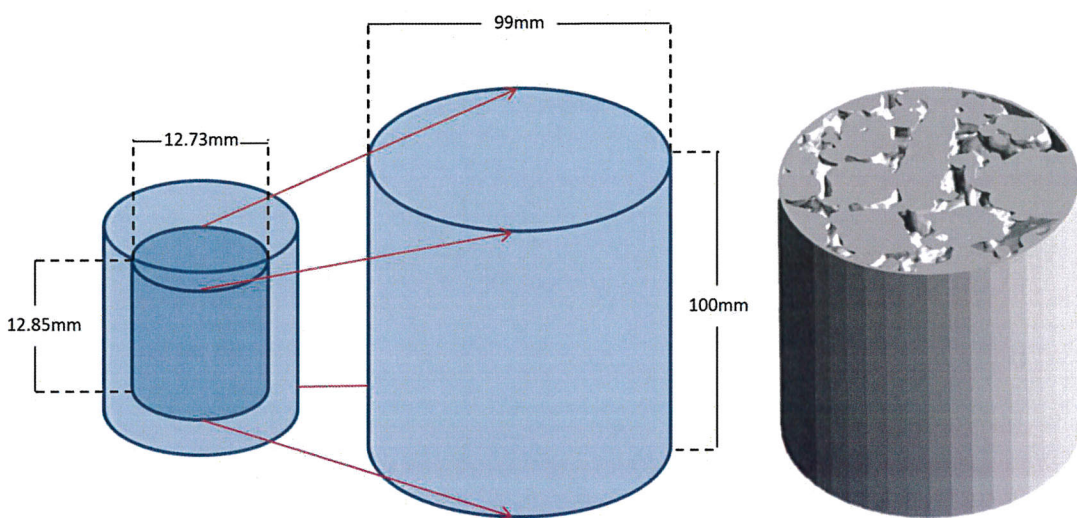


Figure 6 - Scaling of 3D model and Extraction of region for Rapid Prototyping

Selective Laser Sintering (SLS) equipment in the Centre for Additive Layer Manufacturing (CALM) at University of Exeter was used to manufacture the model.⁷ SLS is a procedure of fusing together layers of powder into a 3D model by a computer-directed CO₂ heat laser. 3D CAD data of the component is sliced into layers and the polyamide powder is sintered layer by layer. Additional powder is deposited on to each solidified layer and then again sintered (3t RPD Ltd, 2010). Typically when using ALM, complex geometries are difficult to achieve, however through the use of laser sintering, intricate details and complex internal geometries are possible, making it a very suitable method for modelling soil structure.

The limitation of SLS is that it is not well suited to large, dense solid volumes. In order to ensure the component to be produced would have a high level of accuracy, the internal volumes of the solid phases (representing the inside of filter media particles) were removed. This ‘hollowing-out’ method reduced the volume of material to be sintered but still ensured flow paths and geometry remained intact. A minimum wall thickness of 3mm was assigned to the model to guarantee internal strength.

A second model was created from ALM, not for the purpose of flow testing, but instead as a means of physical visualisation of the micro-scale porous networks present in the media. This model was created as a ‘reversal’ of the 1st model, with the porous zones represented as solid matter and the filter media/solid volumes left as space. This invert model had a much smaller solid volume than the 1st model, and as such required no hollowing of the solid phases.

The compact, ‘Formiga P100’ machine was used to make the models. This equipment is capable of creating components directly from CAD data and allows modelling of the samples in a turnover time of 8 hours. Under the build conditions, the smallest detail that the machine could produce was 0.1mm, with scaling this gives details representative of 13μm in the original sample.

After the SLS process had completed, the models were thoroughly cleaned using an air hose to remove any un-sintered powder. This was important to ensure the internal volume of the sample was clear of additional powder prior to any further testing.

5.6. Phase 7: Flow tests on Rapid Prototype sample

Experimental Setup

The experimental rig used for testing is based on that used by (Baker & Tabor, 2010) and (Tobis, 2000) to investigate flow through packed beds⁸. This method was chosen as the CFD models created were based upon theory of packed beds, and by using a corresponding experimental method, direct validation of CFD results could be made. Furthermore, the investigation requires a method measuring pressure difference, volumetric flow rate, velocity and Reynolds number, all of which can be measured through implementation of this experimental setup. Pressure drop across the sample length was found experimentally for a range of superficial flow velocities. Air was forced through the additive layer manufactured sample using a centrifugal pump.

Experimental pressure drop over the sample length was calculated by means of a differential micro-manometer, with pressure taken at points at a spacing 30mm, immediately before and after the sample. In order to ensure that the pressure readings were representative of the average over the cross sectional area, two pressure outlet points at the same level were used both before and after the sample.

⁷ Ed James, Specialist Engineer of CALM conducted the Rapid Prototyping and kindly secured funding for the material and operational costs.

⁸ Testing apparatus provided by Dr. MJ Baker

The flow rate was controlled using a flow plate that could be manually adjusted across the flow pipe cross section to increase/decrease flow through the system. The superficial velocity, was measured downstream of the sample using a hot-wire anemometer. Testing was initially conducted with a pitot static tube attached to a differential manometer, however using a hot-wire anemometer gave smaller fluctuation in readings.

In initial tests, large fluctuations in the recorded velocity gave very sporadic results. This was deemed to be due to unsteady flow conditions downstream of the sample. A section of honeycomb tubing was manufactured and installed downstream of the testing area in order to create a more linear flow pattern and reduce the unsteady flow.

40 Flow tests were conducted on the ALM filter media sample, in 2 testing runs, with pressure drop readings calculated for 20 different increments of superficial flow velocity, in the range of 0.1m/s to 1m/s. The same testing procedure was carried out on the packed bed sample provided by Dr. Baker (Baker, et al., 2011). The packed bed sample consisted of 164 uniform spheres, in a random packing formation, with a bed porosity value of 0.48 (image of sample shown in Appendix E). The testing on both samples would allow a comparison of the filter media to the packed bed behaviour. Due to small fluctuations in both pressure and velocity readings, averages from 5 reading at 4 second intervals were taken for each flow test. Using thermometer measurement within the testing chamber, the flow temperature was found to be 22°C. Air density ρ was taken to be 1.2kg/m³. Figure 7 below shows a diagram of the experimental setup. Photos of the experimental rig and sample tasting can be found in Appendix E.

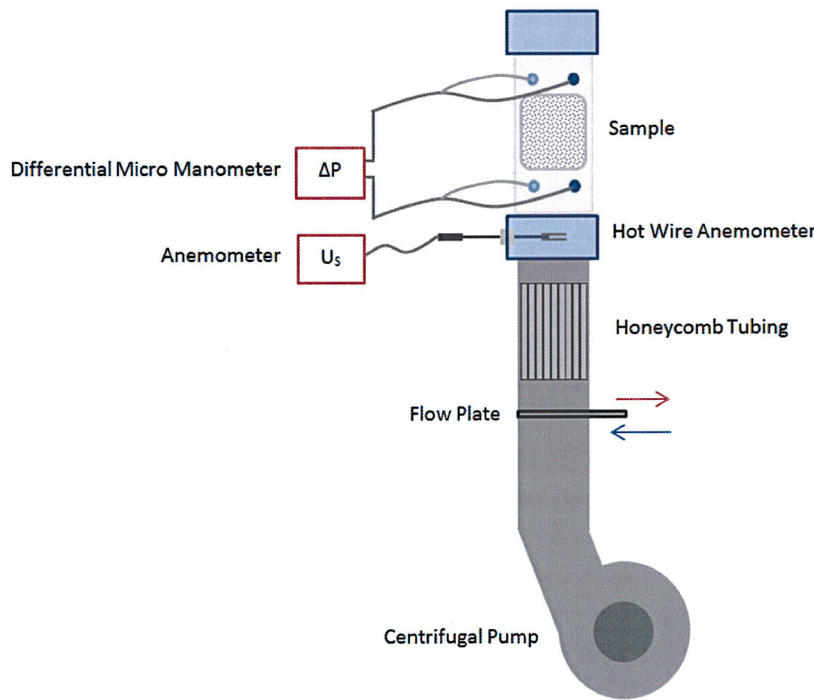


Figure 7 - Experimental Setup for Flow Tests

5.7. Phase 9: Attenuation investigation

This phase of experimentation was conducted to look into the ways in which micro-CT investigation can be used not only to retrieve pore space micro-architecture but also allow the characterisation of the distribution of different materials within natural samples. Extensive research has been conducted into the identification of materials within samples that have AC

values which vary by large magnitudes, and segmentation into different material phases (metal/air, bone/blood vessels) can be conducted with relative ease based on AC values. With natural materials such as soils, where materials are of similar densities and chemical structure, the X-ray AC values are of the same order of magnitude, and as such, the segmentation into different phases is more complicated.

Data obtained from phases 3 and 4 was analysed using the program 'VG Studio Max 2.1'. The raw tomographic images obtained consisted of a 3D array of reconstructed 16-bit x-ray AC values that were related to the density of the material being scanned. Using the greyscale histograms of the reconstructed volumes, investigation into the identification of local minima between peaks was conducted to establish thresholds which could be implemented to allow segmentation of the image into different material phases.

5.8. Health and Safety Considerations

With a number of different experimental techniques being used in the investigation, it was important to identify the health and safety considerations associated with the apparatus, processes and materials involved. Risk assessments for the experimental procedures and site visit undertaken can be found in Appendix F. The primary health and safety considerations surrounded the use of the micro-CT scanner and the site visit.

Exposure to potentially harmful radiation when operating and working with micro-CT scanners is a risk that must be acknowledged and considered within the laboratory (Maharaj, 1994). Systems are incorporated into the equipment to prevent and reduce potentially adverse health effects. The door of the testing chamber of the machine is connected through a locking system with the x-ray source, preventing the source from operating unless the testing chamber is secured with the door in the closed position. Operation of the equipment is only performed by trained, experienced staff. Dr. Lesley Wears carried out the scanning of the samples and adhered to necessary health and safety regulations of the laboratory.

For any site visit it is important that all parties involved are aware of the potential risks of the environment in which they are working. The site in Barry, South Wales was an active car park, with traffic access to the area throughout the day. In order to ensure the group members could work safely, high visibility jackets were worn at all times and careful attention was paid to the public using the area. When sampling filter media from the bioretention units it was necessary to remove the heavy steel grating. This task was undertaken by the members of *Hydro Int. (UK)*, and all individuals present wore steel toecap boots when working around the units. Prior to the site visit, a full risk assessment was completed, see Appendix F.

6. Results & Discussion

6.1. Phase 2:

A CT image of the fine-gravel sample from the initial sample set is shown in Figure 8. An example of the raw x-ray image for the scan is shown in (b). After reconstruction and post-scan modification to remove any significant artefacts, the results of the scan were generated in 2D (b), (c). With the long scan time (~90 minutes) the scans obtained a voxel size of 0.0262 mm³. Using *CT Pro 3D* the 2D images were combined to create a 3D volume rendered model.

Figure 8 (d) shows a snapshot of the 3D tomographic model for the fine-gravel sample, with a cutaway section. Full size versions of the scan images for the 3 samples are included in Appendix C.

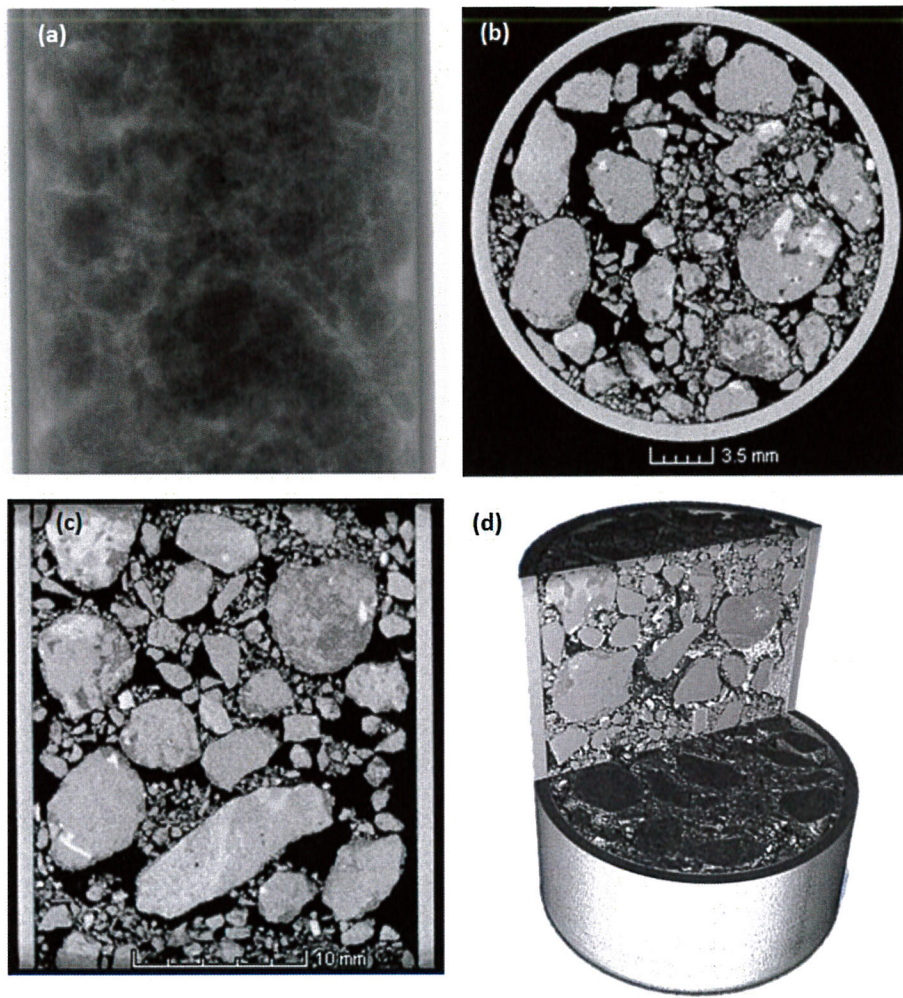


Figure 8 - Scan images for 'Fine-Gravel' (sample #1) from initial scan samples

The results obtained show very clearly the spatial distribution of the granular material within each sample. There is a defined contrast in the imaging, allowing distinction between the solid matrix and the surrounding pore space. This is due to the fact that the sample material is very homogenous, with two materials present in the sample; air and gravel. When a volume was extracted from the scan to remove the glass tubing section, the AC grey-scale histograms were very clearly bimodal, with a peak originating from the solid matrix and another from the pore space. This was the case for all samples from this initial phase as in each case the sample had been prepared from one sample material. In the case of the filter media, the presence of compounds with differing density makes the segmentation into these two clear phases more complicated. The original scans conducted as part of testing in phase 1 did not have the level of detail shown in this set of results, indicating that the longer scan times, and greater number of projections makes a significant improvement in image quality. These scans show a level of detail that allows the identification of the porous networks, particularly in the case of the coarse samples (#1 and #3), making them well suited to further use in CFD mesh creation. Another observation that can be made from these scans is the effect of particle size on the porosity. The samples with coarse, larger grains (#1 and #3) have much larger pore spaces, often with pore channels that measure a visually estimated 4 or 5mm in diameter. The scans highlight the fact that with an increase in grain size and resultant surface area, the porosity is significantly increased. The 'fine sand' sample (#2) has a much smaller particle size than the other two samples, and the resultant dense packing visible in the micro-CT images shows an visually assessed lower porosity than the coarse samples.

6.2. Phase 3/4:

Different cutaway views of 3D volume reconstructions of the 'Hydro Lab Sample' and 'Case Study Sample' are shown in Figure 9 and Figure 10.

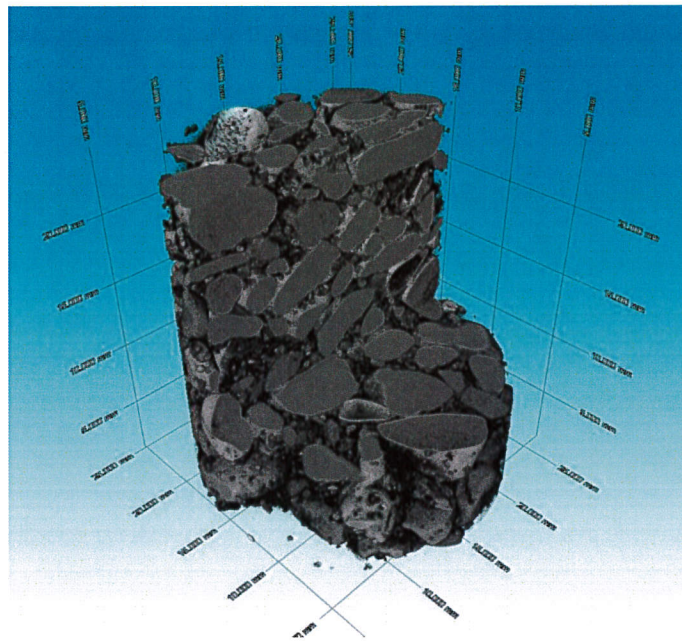


Figure 9 - Cutaway view of 3D volume reconstruction - 'Hydro Lab' sample

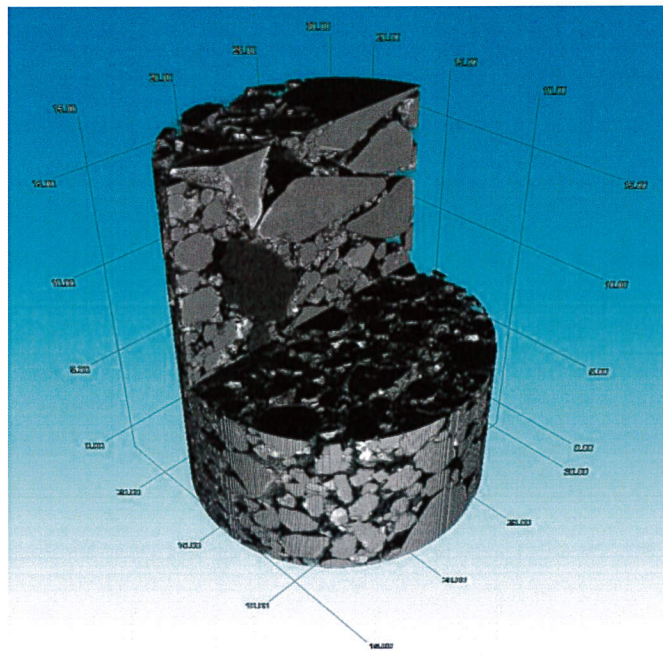


Figure 10 - Cutaway view of 3D volume reconstruction - 'Case Study' sample

The scanning time in each case took ~90 minutes. After post-scanning processing the degree of artefacts and noise was low. The scan of the Hydro Lab sample gave a voxel size of $22.73\mu\text{m}$. This high resolution allowed a very clear visualisation of the pore space at high levels of magnification. The data from the scan was passed to the CFD team for IBM. Feedback regarding the results of this scan from the CFD team indicated that the data could be well applied to the meshing technique, however a higher resolution scan with a smaller

voxel size, if achievable would increase accuracy. From visual inspection prior to scanning it was apparent that the Case Study sample had a finer particle size than the Hydro Lab sample (later verified experimentally Section 6.3), and as such it was decided to scan a second sample, with a smaller diameter of sample container, in order to achieve a smaller voxel size and greater detail from the scan. A tube diameter of 19mm was scanned and the results gave a voxel size of $10.34\mu\text{m}$. This smaller scan diameter data was used, as it allowed a greater level of magnification and resolution than the bigger sample. This indicates that a reduction in sample diameter gives a much higher resolution, as the x-rays have less material through which they must pass and magnification can be increased.

Porosity

In order to assess the porous structure within the results found, it was first necessary to distinguish between the solid space and pore space. The method adopted used inspection of the AC histogram alongside visual inspection of 2D magnified CT images of regions.

As seen in Figure 11 below, the AC histogram has a very clear local minimum between the first two peaks. Using threshold points (marked by red lines in Figure 11) to create a region, the volume within the thresholds can be displayed visually as a yellow region on the 2D views on different planes through the total sample volume. Adjustment of the position of the lower threshold point and visual inspection of the 2D images indicated that the first peak did not represent solids in the scan; however the second peak did. This showed that the threshold between solid and porous phases lay in the local minimum region between the peaks. Through magnification and inspection of the local minima a point for the threshold was identified as shown in Figure 11. This process was repeated for both samples. Further progressions and analysis of the AC histogram and threshold applications can be found in 6.7.

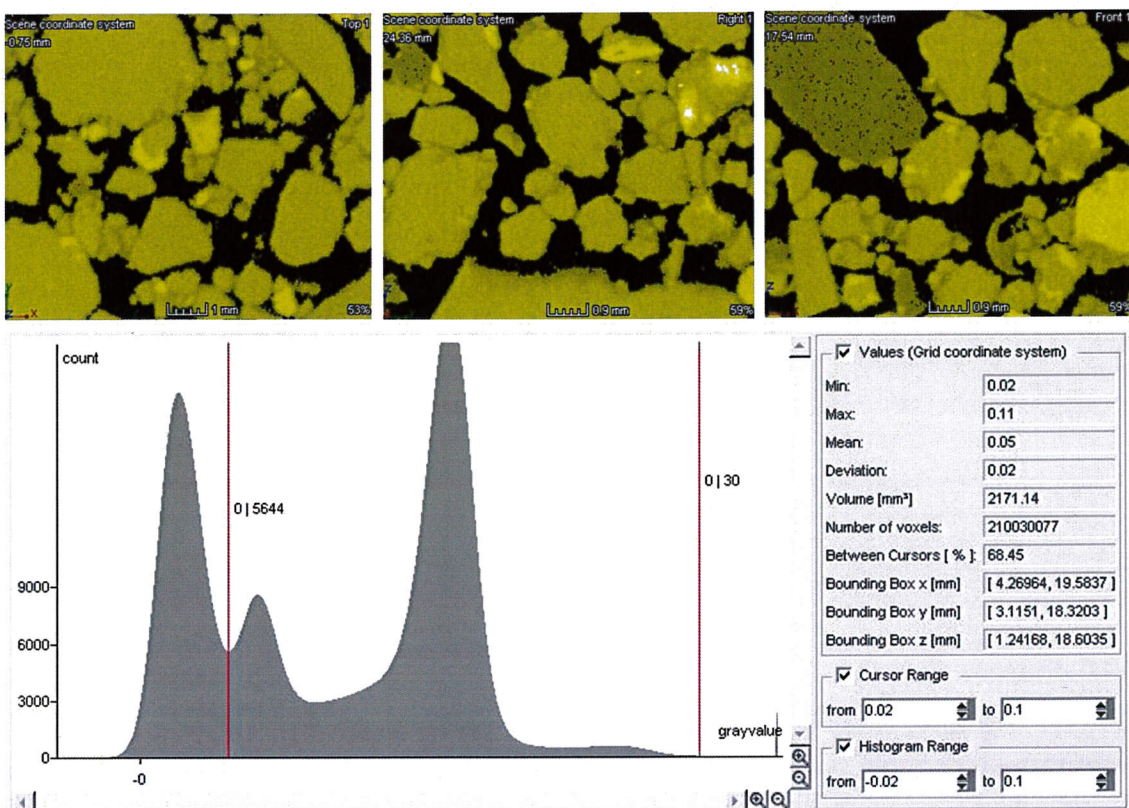


Figure 11 - AC Histogram and 2D Images used simultaneously for pore identification – ‘Case Study’ Sample

As stated in section 2.1, the total porosity can be described as the ratio of the void volume to total volume. Extracting the solid region within the defined thresholds, the percentage of total volume that this region represented could be found. Applying this method of volume analysis to both samples gave the following total porosity values;

Sample ID	Percentage Volume within threshold	(100 - % Vol within threshold)	Total Porosity
Hydro Lab	71.97	28.03	0.2803
Case Study	68.45	31.55	0.3155

Table 1 - Porosity values for 'Hydro Lab' and 'Case Study' samples

It can be seen from Table 1 that the case study sample has a higher porosity than the Hydro lab sample. There are two suggested reasons for this difference between the values. Firstly, it may be due to a lower presence of 'fines' (smaller silt like particles in the filter media) in the case study sample, as the filter media has been in operation for a long period of time, and these finer particles may have been 'washed through' with the repeated wetting of the bioretention system, resulting in larger porous spaces and a higher porosity. This reasoning can however be deemed as unlikely, as the results shown in 6.3 based on sieve analysis show that the case study sample contains a higher proportion of the smaller particles than the Hydro lab sample. The second and more likely explanation for the difference in these values may arise from experimental error. In the case study sample case, the segmentation from the AC histogram can be deemed to be reliable, as there was a clear local minimum that could be identified. In the Hydro lab sample, a clear point did not exist, and defining a threshold was less clear. With this in mind, the result obtained from the case study should be treated as more reliable and may explain the discrepancy in the results.

Whilst total porosity is useful as a characteristic of the filter media, the effective porosity of the sample is of greater importance when applying the parameter to fluid flow. The effective porosity was found by working in collaboration with A.Begley. As explained, the case study sample was deemed to have a higher accuracy for porosity, and as such this sample was used in further investigation. Using the mesh and flow model A.Begley had created from the scan data, the volume through which fluid flow occurred could be found. Comparing this volume to the total volume of the model, a value for the effective porosity was calculated (see Table 2). The report 'I2' (Begley, 2012), states the volume percentage to be 24.97%.

Sample ID	Total Porosity	Effective Porosity	Difference
Case Study	0.3155	0.2497	0.0658

Table 2 - Comparison of Total and Effective Porosity - 'Case Study' sample

This agrees with theoretical expectations (explained in 2.1) as the effective porosity is smaller than the total porosity. The results indicate that 20% of the porous space does not contribute to fluid flow, and is most likely comprised of isolated or non-interconnected pores. It should be noted that in the process of meshing the scan data there is a partial loss in detail as the mesh size is limited and may not account for some of the smallest particle sizes present, resulting in a slight underestimation of effective porosity.

As (Bear, 1972) states "the particle size distribution may appreciably affect the resulting porosity....poorly sorted soils will have a considerably lower porosity than well sorted ones", so it is important to investigate porosity with consideration to particle size distribution.

6.3. Phase 5:

The sieve tests carried out on the three sample media were carried out a number of times. Initial tests gave a percentage cumulative loss of mass of greater than 1%, and as such were repeated until the test procedure was deemed to be of an acceptable accuracy (<1% mass lost during testing) (Budhu, 2007). The final full results for the sieve test can be found in Appendix D. From the standard sieve tests conducted the particle size distribution (PSD) for each sample was found and is shown in Figure 12.

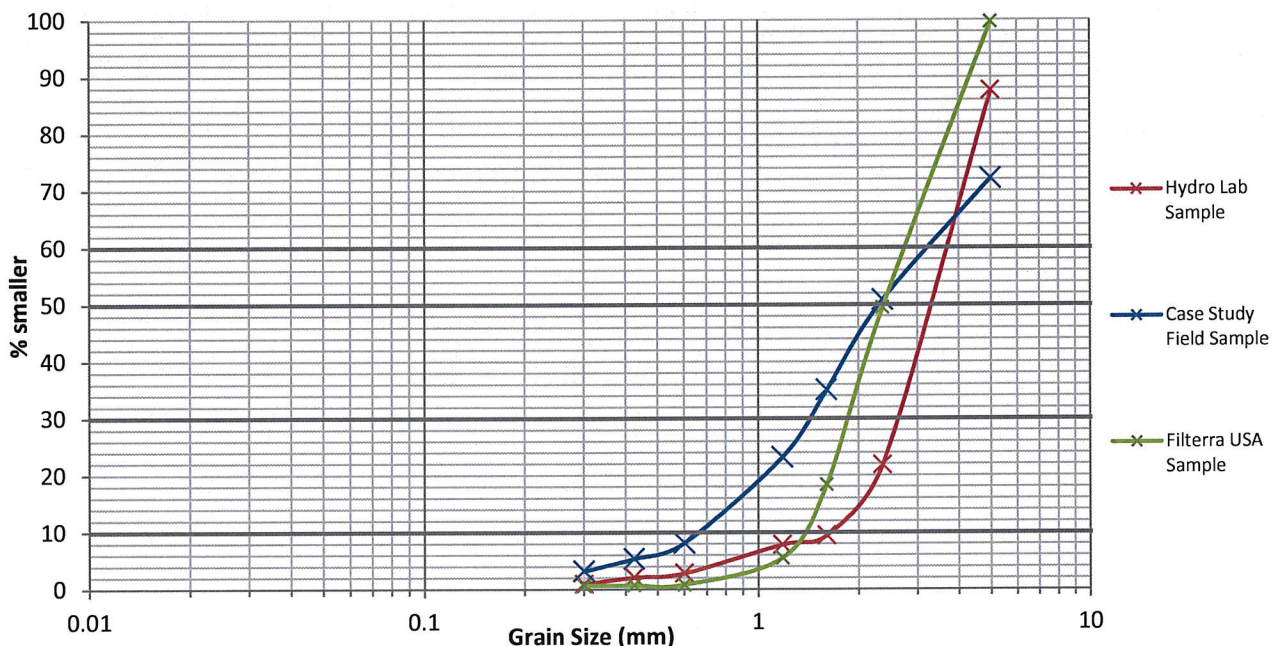


Figure 12 - Particle Size Distribution for 3 sample media

Sample ID				Average Grain Size	Coefficient of Uniformity	Coefficient of Curvature
	D ₁₀ (mm)	D ₃₀ (mm)	D ₆₀ (mm)	D ₅₀ (mm)	Cu ($\frac{D_{60}}{D_{10}}$)	$\left(\frac{D_{30}^2}{D_{10} \times D_{60}} \right)$
Hydro Lab	1.65	2.63	3.68	3.31	2.23	1.14
Case Study	0.66	1.43	3.20	2.30	4.85	0.97
Filterra™ US	1.39	1.86	2.75	2.38	1.98	0.91

Table 3 - Classification figures from Particle Size Distribution

It can be seen from Table 3 and graphical representation in Figure 12, that the Case Study sample has the highest coefficient of uniformity, indicating that there are a wider range of particle sizes present in the sample. The Filterra™ US sample has the lowest value of uniformity coefficient, and has a very small range of particle sizes present. The Hydro lab and Filterra™ US samples can be classed as uniformly graded soils, as Cu<4 (Budhu, 2007). All three samples are narrow graded. The Case Study sample has the highest percentage of fine content, with 3% of the sample mass consisting of particles smaller than 0.3mm. Both the

Hydro Lab and Filterra™ US samples have very little organic content, and are less well-graded. All samples of the filter media can be classed as Coarse Sand/ Fine Gravel according to British Standards for sieve test and soil analysis.

After the sieve testing had taken place, following discussion with *Hydro Int (UK)* it was made clear that there were concerns that the filter medium supplied ('Hydro Lab' sample), may not have a sufficient organic content, which agrees with the results found from this sieve testing and PSD analysis.

From the sieve testing, the D_{50} value is of interest for a number of applications within the group testing. The D_{50} value represents the median grain size. With the application of packed bed theory to porous media flow used in latter stages of the group investigation, the median grain size can be taken to be representative of the average particle diameter, termed D_p , for use in CFD and other flow model theory.

The 'effective grain size' D_{10} is an important factor in flow resistance within the porous network. The calculated D_{10} values for the different samples can be used in Hazen's formula to directly estimate hydraulic conductivity. Whilst Hazen's formula is typically used for sands and loosely packed soils; all the samples fit in the valid range; with D_{10} ranging from 0.1-3mm and $Cu < 5$, allowing the equation to be used as an estimation and guide for permeability of the different media. The Hazen's coefficient used in this case is 0.4: the figure in accordance with 'sandy-gravel' reported by (Lambe & Whitman, 1979). Results and discussion can be found in Table 4, section 6.6.

6.4. Phase 6:

The ALM of the model extracts was very successful, with models created that allowed a clear physical representation of the inner structure of the porous network. Upon visual inspection the 2nd model showed a number of larger porous networks through the model and many small interconnected zones between these larger spaces. Whilst the SLS process uses discrete layers, the level of detail was very high, with no apparent loss in detail, and smooth edges and faces throughout. Figure 13 below show the final samples created using ALM.

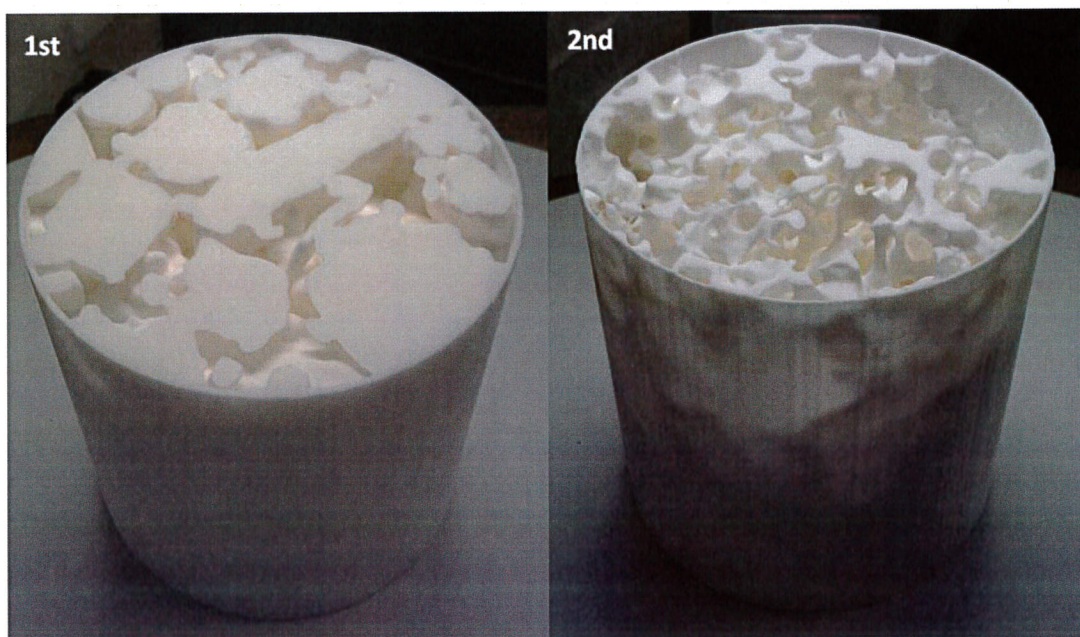


Figure 13 - Final models created using Additive Layer Manufacturing - 1st Solid Particle Domain, 2nd Pore-Network Domain

6.5. Phase 7:

The full results of the flow tests conducted on the ALM scaled model of the ‘case study’ sample media and on the other ‘packed bed’ sample (Baker, et al., 2011) can be found in Appendix E, along with photos of the experimental procedure. During testing, with the addition of the honeycomb tubing within the flow channel, the fluctuations in the anemometer readings were typically small ($\pm 0.02\text{m/s}$), and the fluctuations of micro-manometer reading were smaller still (typically $\pm 0.01\text{mbar}$). The results displayed graphically represent averages of five readings for each superficial velocity increment.

The graph below (Figure 14) shows the pressure drop per unit length (Pa/m) for a number of given superficial flow velocities (m/s) recorded over the course of two testing runs. The secondary x-axis represents the particle Reynolds number (Re_{dp}) of the flow. The average particle diameter used in the calculation of Re_{dp} is 17.86mm, found from the D_{50} value of the ‘case study’ sample (see 6.3 above) multiplied by the scaling factor used in the model.

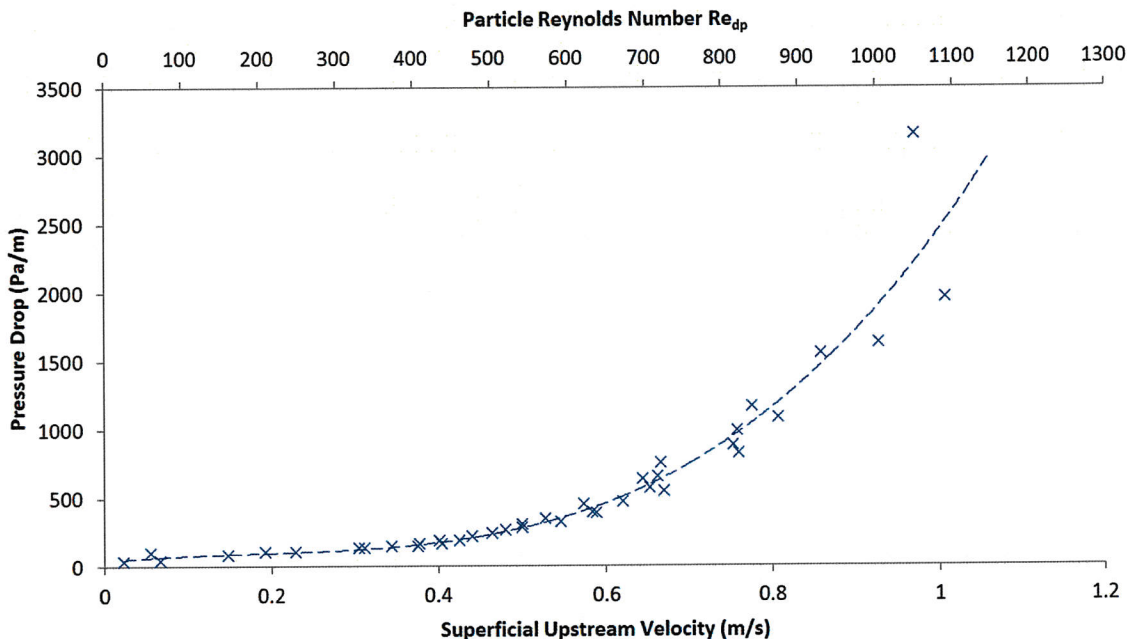


Figure 14 - Graph of Pressure drop per length VS Superficial Velocity and Particle Reynolds Number - For ALM 'Case Study' Sample

It can be seen from the graph that as the superficial velocity (and corresponding flow rate) is increased, the pressure-drop across the sample increases. Darcy’s Law indicates that the relationship between these two measured parameters follows a linear trend; however the graph has a quadratic or cubic relationship over the range of velocities investigated. This is due to the region of validity of Darcy’s Law (typically for laminar flow at slower velocities), and one can deduce from these experimental results that analysis of the laminar region is necessary to assess Darcy’s Law. As stated in the theoretical section 2.3.4, the flow can be characterised as laminar ($\text{Re}_{dp} < 10$), transitional ($10 < \text{Re}_{dp} < 300$) or turbulent ($\text{Re}_{dp} > 300$). The dimensionless particle Reynolds numbers for both the ALM filter media sample and packed bed sample are plotted against pressure drop per length on a logarithmic scale in Figure 15 below.

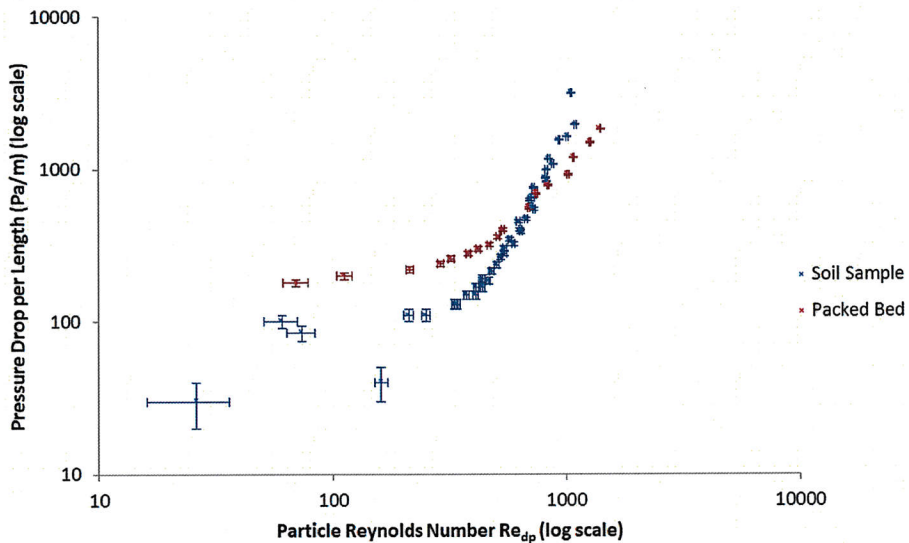


Figure 15 - Graph of Pressure drop VS Redp for 'ALM filter media sample' and 'packed bed sample' (log scale)

The results show that at particle Reynolds numbers lower than ~ 300 there is no clear trend in the data, particularly for the ALM filter media sample. Increases in superficial velocity do not correspond with increases in pressure drop across the sample. It is clear to see from this data that in the transitional flow region, where $10 < \text{Re}_{dp} < 300$ (Baker, et al., 2011) (Ziolkowska & Ziolkowska, 1988), the experimental results should be treated as unreliable. Once the flow is fully turbulent, the data follows a more uniform trend. The main source of this experimental error at lower Reynolds number can be accredited to the measurement instruments used in the testing. The micro-manometer and anemometer used have an accuracy of $\pm 0.01\text{mbar}$ $\pm 0.01\text{m/s}$ respectively. Over a sample length of 100mm instrument errors correspond to $\pm 10\text{Pa/m}$ (displayed graphically through the error bars). With this degree of accuracy, it is apparent that the micro-manometer and anemometers are designed for application at higher flow velocities and corresponding pressure drops such as those investigated in the turbulent range of the testing flow rates, as such the inaccuracies at low Reynolds numbers are too high to consider these data readings as valid.

In order to assess whether air flow through the porous network of the filter media micro-architecture is analogous to flow through a packed bed it is necessary to directly compare the experimental results with packed bed results in a dimensionless manner.⁹ The graph below (Figure 16) shows a dimensionless comparison between the results of the ALM filter media sample and packed bed sample. The theoretical 'Ergun equation' and 'Eisfelds & Scnitzlein equation' have been plotted to give a representation of the expected behaviour of a packed bed (Begley, 2012) (Pavey, 2012). The equations have been plotted for each of the samples, using the same values of average particle diameter as before, and a value of porosity of 0.48 for the packed bed sample (Baker & Tabor, 2010), and 0.2487 for the filter media sample (Table 1).

⁹ By using dimensionless pressure drop φ and particle Reynolds number Re_{dp} the experimental data can be directly compared to results from other packed bed flow tests with other dimensions, porosities, and average particle sizes.

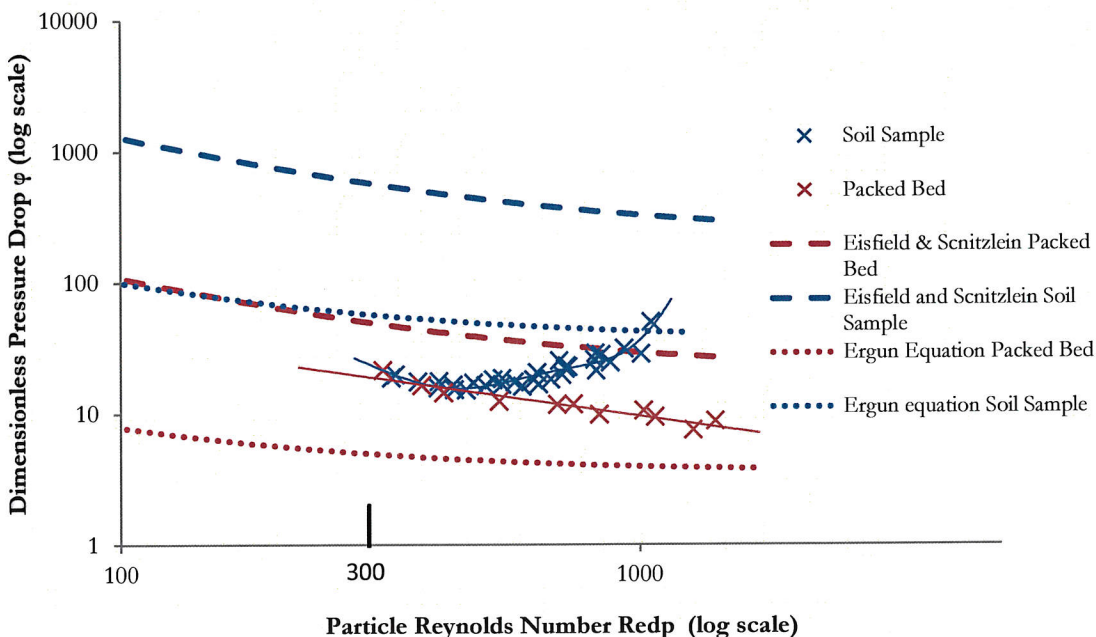


Figure 16 - Graph of dimensionless pressure drop VS particle Reynolds number for ALM sample and packed bed sample, with theoretical trendlines based on Ergun and Eisfield & Scnitzlein equations

It can be seen from the graph (Figure 16) that the results for the ALM filter media sample do not follow the theoretical or experimental trends for air flow through a packed bed. The experimental results from the packed bed sample show a decrease in dimensionless pressure drop with an increase in particle Reynolds number, and whilst the values do not directly compare to the theoretical calculations, they show the same trend. It can be deduced from these results that the air flow through the ALM filter media sample cannot be treated as analogous to air flow through a packed bed.

6.6 Phase 8: Comparison of Results

Table 4 - Comparison of Hydraulic Conductivity estimated from PSD using Hazen's Law, Experimental permeameter results courtesy of L. Whitehurst, and CFD models courtesy of A. Begley

Sample ID	D_{10} (mm)	Estimated Hydraulic Conductivity k (cm/s)	Experimental Hydraulic Conductivity k (cm/s)	CFD Hydraulic Conductivity k (cm/s)
Hydro Lab	1.65	1.089	0.112	2200
Case Study	0.66	0.174	0.133	350

As shown in Table 4 above, the hydraulic conductivity values calculated from Hazen's equations, based on the PSD of the samples are higher than the results found experimentally through permeameter tests conducted by L.Whitehurst. The estimated value for the case study sample is a close approximation of the value obtained experimentally, however the Hydro lab sample estimation is an order of magnitude too large. The findings of (Sperry & Peirce, 1995) indicate that whilst the Hazen equation is the most suited estimation for granular sands/gravels, the theoretical results are for the most part larger than the experimental values recorded, as seen in this project. When the values are compared to those from A.Begley, obtained by solving the CFD models, there is a difference of a number of orders of magnitude. The factor of difference between the case study and Hydro lab samples is 6.3 for

both the estimated values and the CFD model. Whilst the magnitude of the values from the CFD model are several orders of magnitude too high, the relationship between the change in effective grain size (D_{10}) and change in hydraulic conductivity (k) agrees directly with Hazen's Law.

The results from phase 7, outlined in 6.5, can be compared with results from A. Begley and S. Pavay, to validate the micro-scale CFD and homogenous region models constructed and solved as part of the CFD group work. As stated in 6.5, the results from flow tests disproved the assumption of analogous behaviour with a packed bed. As such, using particle Reynolds numbers and dimensionless pressure drops based on packed-bed theory was not a valid method of comparison for the models in question. To allow validation, the flow conditions and dimensions in the CFD models were matched to experimental conditions, whilst maintaining the mesh geometries, allowing comparison directly from calculated superficial velocities and pressure drops (Begley, 2012) (Pavay, 2012). The three sets of results are shown on the logarithmic graph in Figure 17.

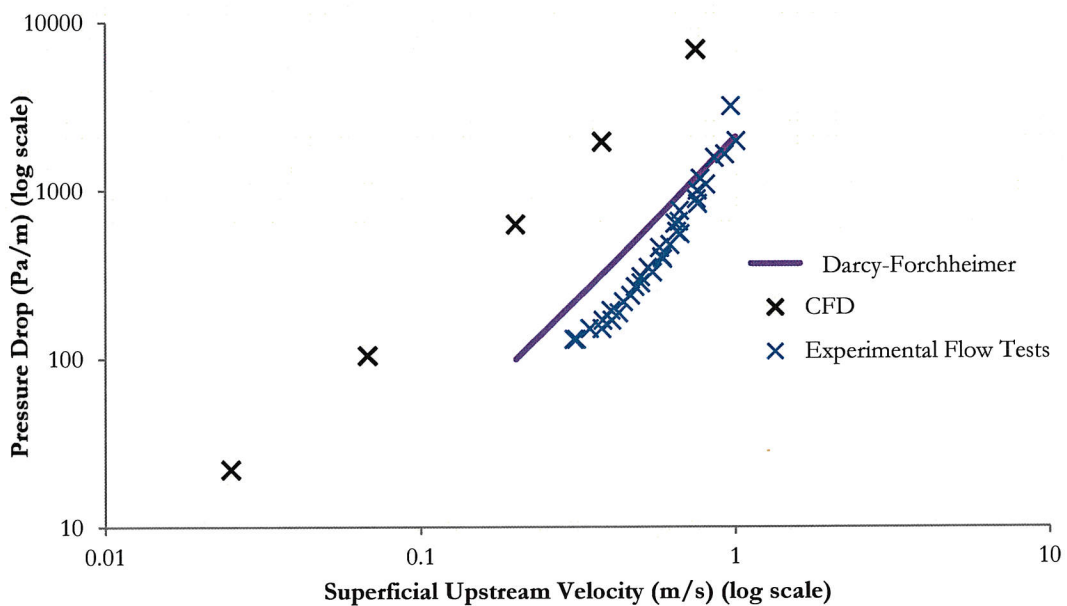


Figure 17 - Graph comparing pressure drop/superficial velocity results for Darcy Forchheimer, CFD models, and ALM Model Flow tests

It can be seen from the graphical comparison that the three sets of results follow a similar trend. In all cases there is a quadratic relationship between superficial velocity and pressure drop per unit length. The results from experimental results show strong similarity with the Darcy-Forchheimer theoretical results. There is a strong agreement in trend between the Darcy-Forchheimer theoretical results and the CFD results. However, the CFD results yield pressure-drop figures that are too large by an order of magnitude. The CFD results also display this overestimation when compared to the hydraulic conductivities (discussed above), although the graph in Figure 17 shows the disparity with the Darcy-Forchheimer values is of a constant order of magnitude.

As explained by (Begley, 2012), it can be seen from the two comparisons that the CFD model yields results that correspond to theoretical expected behaviour but output results that are in some cases several orders of magnitude to high. This may be due to limitations in the meshing and CFD approach adopted, or a result of the exclusion of a turbulence model.

The experimental results from the flow tests conducted show strong similarity to those obtained by S. Pavay. Whilst the two sets of data do not fully agree, (Pavay, 2012) explains

that small variations of the average particle diameter and/or porosity values used in the theoretical calculations yield large changes in the resulting pressure drops. This indicates that experimental errors in the sieve testing and imaging phases and resultant inaccuracies in the porosity and mean particle diameter significantly affect this data.

6.7 Phase 9

The AC histograms from the micro-CT data in 6.2 were extracted and assessed using *Matlab*. When plotted independently the histograms were on differing scales, by a number of orders of magnitude, due to the scan settings applied. Both sets of data showed a number of peaks, with two distinctive larger peaks apparent in both sets (shown as 1 and 2 in Figure 18 below). These two peaks were accredited to the corresponding voxels containing air (1), and higher-density filter media material (2). By matching these two peak positions, which are assumed to have the same relative attenuation in both scans, and using the linearity of the AC scale (see 3.1.1), the two graphs could be normalised through mathematical scaling, and hence plotted on the same axis for direct comparison.

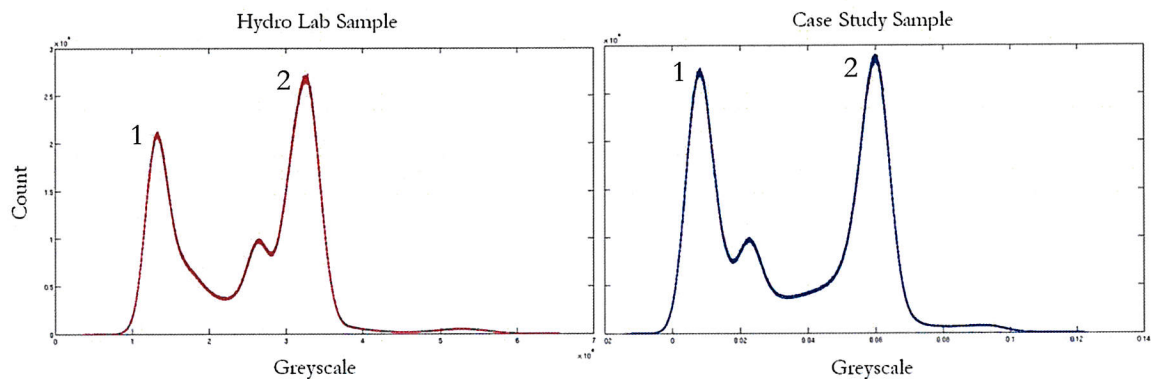


Figure 18 - Greyscale Attenuation Histograms for scanned samples

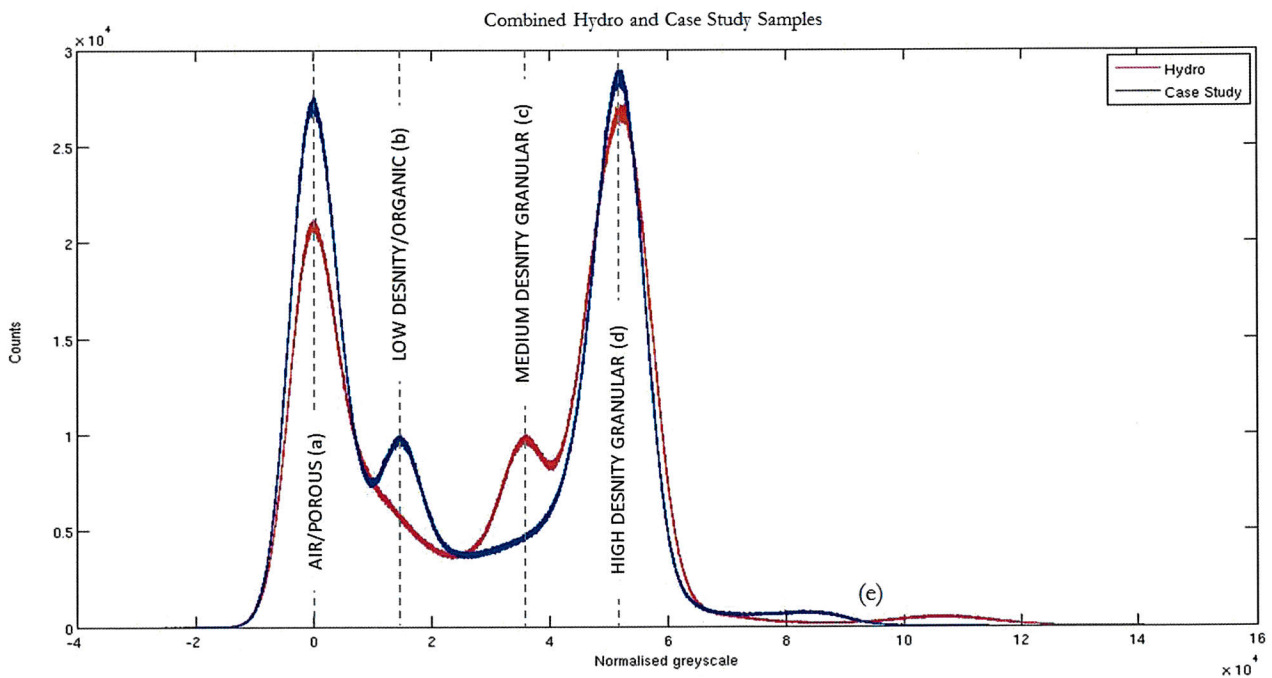


Figure 19 - Normalised Greyscale Attenuation Histograms for scanned samples

From comparison of the two AC histograms it can be seen that there are four clear, localised zones of AC greyscale coefficients that can be identified through the presence of peaks on the graph. These have been indicated by a, b, c, d and e shown in Figure 19. Investigation into each of these peaks, and the local minima is conducted to obtain five phase separation of the image and subsequent 3D volume.

Given the linearity of the CT process in the reconstruction from AC values, the spacing between the peaks demonstrated on the greyscale axis used can be assumed to be directly proportional to the differences of AC values of the materials they represent. From research, and discussion with *Hydro Int. (UK)* it is known that the filter media mixes comprise of a mixture of fine gravel substances and organic (soil) content. If the first of the peaks identified is excluded and considered as the gaseous phase representing air, then it is observed that the solid component of the filter media is comprised of four phases.

The organic content has the lowest average density of the solids present, and can be identified as the material corresponding to the AC value represented as the peak marked (b) in Figure 19. By identifying the local minima that bound this peak and applying thresholds for each sample, the volume containing voxels with AC values in this range was extracted and rendered using *VG Studio Max*. The results of this process are shown in Appendix A.

The case study sample displays a large number of voxel counts for this attenuation; however the Hydro sample has a much lower proportion of organic content. This agrees with the PSD results in 6.3. Through inspection of the 3D volume rendered model the organic layer is identified as a ‘coating’ around the higher density gravel particles. It can be induced from this presence of this organic content that diameter of porous zones is reduced, affecting the hydraulic conductivity through the media.

It is apparent from Figure 19 that the Hydro sample does however have another peak corresponding to an AC level higher than the organic content, labelled as region (c). Through the same thresholding operation as defined above, close examination of the 2D and 3D CT images of this region indicate that the material in this volume represents far larger grains than the organic content, with similar size and shape to the abundant high density gravel present. It is assumed from this that the material represented in these volumes is a granular gravel substance of a medium density, and not organic/fines. It is present and identifiable in the Hydro sample, but represents a very small volume in the case study sample and is difficult to extract and define as a phase in this case. The extracted volume from this region and volume rendered models for the Hydro sample can be found in Appendix A.

The region represented by the peak (d) is the most abundant of the solid phases. This phase can be categorised as the gravel content of the filter media, as the high AC greyscale value corresponds to a material with a high density. Visual inspection shows this phase as large, granular volumes, and material within this phase accounts for the majority of the solid volume. Using the thresholding technique, and extraction of this region, it was found that in the Hydro lab sample this material accounted for 64.4% of the solid volume. Difficulties in segmentation of this region from region (c) in the case study sample did not allow an accurate corresponding volume calculation. The extracted volumes from this region and volume rendered models can be found in Appendix A.

The region indicated by the marker (e) only accounts for a very small percentage of the solid volume in both samples. When examined this region was shown to represent a small number of granular particles located at random dispersed points within the sample volume. Using the linear scale of the AC greyscale histogram it is noted that these particles have a far higher density than the other materials present and as such are assumed to be small quantities of rock or stone material within the sample.

Using the processes outlined above, the methods of image segmentation have been introduced and successfully used to identify and extract volumes of different materials within the filter media sample. In Figure 20 below, the separated phases have been reconstructed in the complete sample volume to represent the application of the process. This is by no means an exact process, as the segmentation of the different phases does leave a certain amount of 'overlap' due to difficulties in phase isolation. In order to improve segmentation of phases, applying a filter during scanning and methods increasing contrast could be used to enhance the peak separations within the histograms. As a further extension task within the project, the scanning was not conducted with this as a primary aim, and as such the scanning protocol would require further refinement to allow improvements.

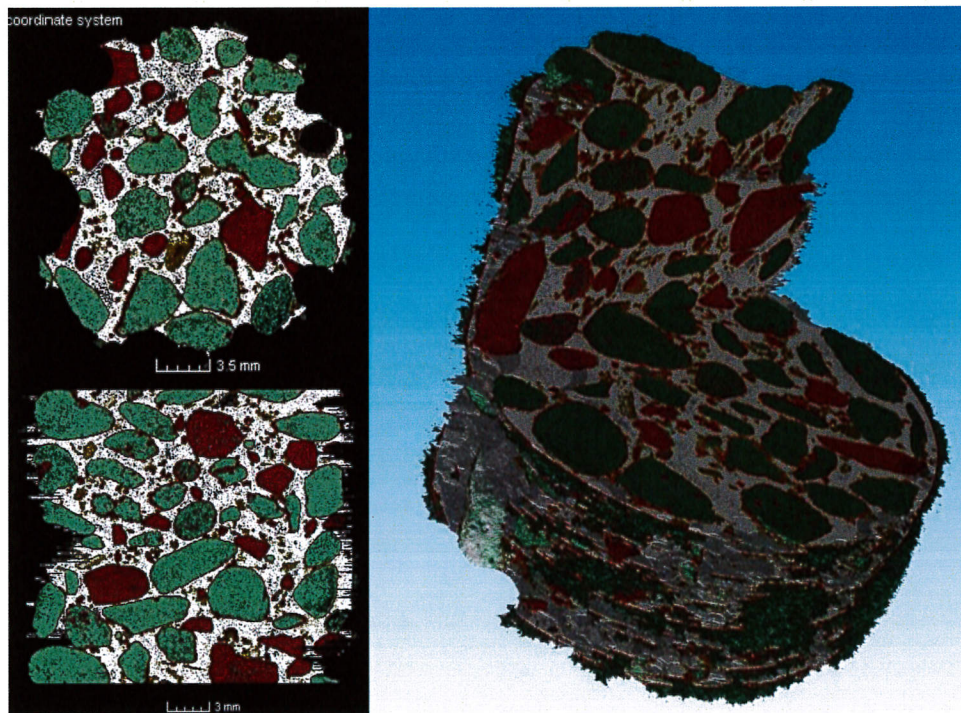


Figure 20 - 3D Volume Rendered image of Hydro Sample following Phase Segmentation

7. Conclusion

The theoretical discussion and experimental undertaking in this project have shown the successful application of X-ray 3D imaging techniques to investigate the internal geometry of granular soils. Through the application of micro-CT techniques, detailed geometries and subsequent 3D models were created to both visualise microarchitecture and examine fluid flow through the porous zones.

The geometrical CT data provided to the CFD group members allowed the successful IBM and construction of a number of CFD models, with a high degree of geometrical accuracy. Using fluid flow volumes in these models, the effective porosity of the filter media was compared with the total porosity calculated directly from the micro-CT 3D volume rendered reconstruction. Results agreed with theoretical expectations and showed the effective porosity to be significantly lower than the total porosity. Due to the inaccuracies of the segmentation process of the micro-CT image, accurate values of porosity were difficult to obtain, however further refinement of the segmentation process as illustrated later in the project may allow improvements in the determination of this parameter.

From the constructed model, an extracted central region was up-scaled using ALM processes. The two models produced allowed a very clear physical method of visualisation of porous configuration of the filter media.

Dimensionless analysis of results from flow tests conducted on the ALM reconstruction indicated that flow through the porous network within granular soils was not analogous to a packed bed made up of spheres. It is suggested that this dissimilarity can be attributed to the tortuosity; the way in which the shape of particles in a porous medium significantly affect flow. Whilst the results obtained did not correspond to those from packed bed tests, they gave a good method of validation for the CFD models and verification for other group members. The validation comparison with CFD results (A. Begley) and theoretical results (S. Pavay) showed that the CFD model was not valid for the range of superficial velocities investigated, however the theoretical results showed good correlation throughout the range. These results were instructive as they provided a strong reasoning as to why the CFD models produced did not give representative magnitudes, particularly at higher flow rates. The models had been constructed based on an assumption of analogous behaviour with packed bed theory (Baker, et al., 2011), and as such did not include a turbulence model. However, the findings of this project indicate that a turbulence model may be necessary in this case.

From sieve testing data it was concluded that there was a significant degree of variation in the distribution of particle sizes between the various samples of filter media. In particular, the 'Hydro Lab' sample, provided by *Hydro Int. (UK)* had a far lower organic content than the sample from the case study *Filterra™* unit. This was corroborated by results in the image segmentation phase of micro-CT analysis. It is suggested that this high content may be due to the presence of the plant/root system, whose active, biological processes replenish and regulate organic matter throughout the filter media volume. From visual inspection of the distribution of the organic volume through the sample, the presence of organic content is deemed to significantly affect fluid flow within the filter media volume.

Further to the initial aims of the project (Please, 2011), investigation was conducted into the process of segmentation of micro-CT image data to differentiate between different solid phases in sample volumes. The preliminary work indicated that using the linear AC scale represented with greyscale values allowed the identification of local peaks and minima, which used alongside visual-based thresholding methods, allow image segmentation into a number of phases. In the case of the filter media studied, the differentiation was difficult due to non-substantial differences in AC values of the materials present. However, it is suggested that improvements could be made by scanning the isolated materials prior to scanning of a collective volume. By matching image data within banded phase zones, the image could be segmented into discreet phases. During the latter stages of completion of this project, an article was published showing further developments of this principle with application to synthetic powders (Mutina & Koroteev, 2012). The findings showed that segmentation of images based on materials with similar AC values was possible. Whilst the investigation was more detailed, the published work follows a method based on the same principle as presented in this paper; utilising the multi-peak greyscale histogram and isolation of local minima. This is a potentially effective method of non-destructive material investigation, which with further work and refinement, could find solicitation in a range of geoscience applications.

8. Recommendation of Future Work

The methods and experimental procedures used in this project were not classical techniques, and are the subject of on-going research and development and their potential for future application has been clearly demonstrated. To further this investigation, the refining of the micro-CT procedures for organic application and the segmentation of micro-CT data for different materials based on AC values are suggested. It is recommended that micro-CT scans

are conducted on a range of isolated solid components of filter media or soil, with consistent scan settings. By obtaining linear relationships between the AC values of the solid phases, full scans of a composite filter media could be conducted with identical settings and the various solid components identified simply and accurately. Methods of this nature are in use, however the application to materials with similar ranges of AC values presents challenges that must be met with appropriate modification of experimental imaging technique. By compiling a larger amount of scan data, and investigating the scanning filters that improve histogram separation, eventual discretisation processes may find use in a range of material and geoscience applications.

Furthermore, the findings of this report indicate that organic ‘fines’ that veneer the coarse grains in soils affect the hydraulic conductivity through porous networks. It is suggested that investigation is conducted into the movement of this organic matter during, and after, the wetting of the porous volume. As fluid permeates through the porous volume, pore space is manipulated and the porous architecture altered in some respect. Using a micro-CT imaging technique, it would be of interest to classify whether these geometrical changes during the wetting and drying of the sample volume are permanent, and how they affect fluid flow over time.

Developments in technology have aided understanding, and it is reasonable to assume that further developments in coming years will continue to reveal new characteristics and answer previously unanswered questions. With micro-CT equipment becoming more compact, and more widely available, it is also likely that these methods will become common place within the geoscience field in the near future. The application of computed tomography in the geosciences shows great potential and scope, and where expansion and understanding have previously arisen from the medical sciences, perhaps with this new specialised application 3D imaging results will continue to improve.

9. Project Review

This individual section of a wider group project successfully investigated the use of new experimental techniques for analysing soil and porous media. The methods used throughout posed difficulties due to the unusual nature of their application, but together with collaboration from a number of external parties and on-going work with other group members, the initial deliverables outlined below (Please, 2011) were all realised within the relevant timeframes.

1. Support L. Whitehurst in the design of the permeameter testing apparatus
2. Obtain samples of the media from both *Hydro Int. (UK)* and from the case study and complete full micro-CT scans
3. Use micro-CT geometries to create volume rendered 3D models of the filter media and up-scaled ALM models
4. Complete flow tests on the ALM models and compare results with both packed bed theory and CFD models

Data obtained from scan processes provided invaluable information for other group members, and found effective application in computational models. Comparison between macro-scale hydraulic conductivities from permeameter test and those obtained from CFD data based on the CT geometries showed large disagreement; however this has been shown to be most likely due to errors within the CFD model. Despite these computational difficulties, the process of IBM from micro-CT scanning of granular filter media was completed successfully. 3D volume rendered models enabled the application of ALM to recreate up-sized physical representation of porous architecture with a high level of accuracy.

References

- Americast Inc., 2009. *Filterra Flow Rate Length Verification Study*, s.l.: s.n.
- Anderson, S., Peyton, R. & Gantzer, C., 1990. Evaluation of constructed and natural soil macropores using x-ray tomography. *Geoderma*, Volume 46, pp. 13-29.
- Argonne national Laboratory, n.d. *Porosity Calculations*, Chicago: US Department of Energy.
- Baker, M. J. & Tabor, G. R., 2010. Computational analysis of transitional air flow through packed columns of spheres using the finite volume technique. *Computers and Chemical Engineering*, Volume 34, pp. 878-885.
- Baker, M., Young, P. G. & Tabor, G., 2011. Image based meshing of packed beds of cylinders at low aspect ratios using 3d MRI couple with computational fluid dynamics. *Computers and Chemical Engineering*, Volume 35, pp. 1969-1977.
- Barrett, J. & Keat, N., 2004. Artifacts in CT: recognition and avoidance. *RadioGraphics*, Volume 24, pp. 1679-1691.
- Bear, J., 1972. *Dynamics of Fluids in Porous Media*. 1st ed. New York: Elsevier Publishing.
- Begley, A., 2012. *Individual Report I2*, Exeter: Exeter University.
- Begley, A. et al., 2011. *Investigating Stormwater Filters and Bioretention Systems (G1)*, Exeter: Exeter University.
- Begley, A. et al., 2012. *Investigating Stormwater Filters and Bioretention Systems (G2)*, Exeter: Exeter University.
- Brown, G. O., 2003. *Henry P.G Darcy and Other Pioneers in Hydraulics*. Philadelphia: ASCE Publications.
- Budhu, M., 2007. *Soil Mechanics and Foundations*. 2nd ed. Phoenix: John Wiley & Sons.
- Capowiez, Y., Pierret, A., Daniel, O. & Monestiez, P., 1998. 3D skeleton reconstructions of natural earthworm burrow systems using CAT scan images of soil cores. *Biol Fertil Soils*, Volume 27, pp. 51-59.
- Carlson, W. D., 2006. Three-dimensional imaging of earth and planetary materials. *Earth and Planetary Science Letters*, Volume 249, pp. 133-147.
- Cnudde, V. et al., 2006. Recent progress in X-Ray CT as a geosciences tool. *Applied Geochemistry*, Volume 21, pp. 826-832.
- Dullien, F., 1979. *Porous Media: Fluid Transport and Pore Structure*. New York: Academic Press, Inc..
- European Environment Agency, 2006. *Urban Sprawl in Europe*, Copenhagen: EEA.

- Fredrich, J., Giovanni, A. & Noble, D., 2006. Predicting macroscopic transport properties using microscopic image data. *Journal of Geophysical Research*, Volume 111, pp. 1-14.
- Geosyntec Consultants, Herrera Consultants, 2010. *Technical Basis for High Flow Rate Treatment and Evaluation of Stormwater Quality Performance*, s.l.: Filterra Ltd.
- Gregory, P. et al., 2003. Non-invasive imaging of roots with high resolution X-ray micro-tomography. *Plant and Soil*, Volume 255, pp. 351-359.
- Grevers, M., De Jong, E. & Arnaud, R., 1989. The Characterization of Soil Macroporosity with CT Scanning. *Canadian Journal of Soil Science*, Volume 69, pp. 629-637.
- Heijs, A., De Lange, J., Schouten, J. & Bouma, J., 1995. Computed tomography as a tool for non-destructive analysis of flow patterns in macroporous clay soils. *Geoderma*, Volume 64, pp. 183-196.
- Hydro International, 2011. *Hydro Filterra Mulch Specification*, Clevedon: Hydro International (UK) Ltd..
- Hydro, I., 2011. *Filterra Bioretention System Design Guide*. [Online] Available at: www.hydro-international.biz [Accessed 24 October 2011].
- Lambe, T. & Whitman, R., 1979. *Soil Mechanics, SI version*. New York: John Wiley and Sons.
- Maharaj, H., 1994. Safety considerations and recommendations for analytical x-ray devices from a review of survey data. *Journal of Health Physics*, 66(4), pp. 463-471.
- Masschaele, B. et al., 2001. First results of micro-neutron tomography by use of a focussing neutron lens. *Radiation Physics and Chemistry*, Volume 61, pp. 623-624.
- Mees, F., Swennen, R., Van Geet, M. & Jacobs, P., 2003. Applications of X-Ray computed tomography in the geosciences. *Geological Society, London, Special Publications*, Volume 215, pp. 1-6.
- Mutina, A. & Koroteev, D., 2012. Using X-Ray Microtomography for the Three Dimensional Mapping of Materials. *Microscopy and Analysis*, 26(2), pp. 7-12.
- Narsilio, G. et al., 2009. Upscaling of Navier-Stokes equations in porous media: Theoretical, numerical and experimental approach. *Computers and Geotechnics*, Volume 36, pp. 1200-1206.
- Pavey, S., 2012. *Individual Report 'I2'*, Exeter: Exeter University.
- Petrovic, A., Siebert, J. & Rieke, P., 1982. Soil bulk density analysis in three dimensions by computed tomographic scanning. *SSSAJ*, Volume 46, pp. 445-450.
- Peyton, R., 1992. Applying X-Ray CT to measure macropore diameters in undisturbed soil cores. *Geoderma*, Volume 53, pp. 329-340.
- Pierret, A., Capowiez, Y., Belzunces, L. & Moran, C., 2002. 3D reconstruction and quantification of macropores using X-ray computed tomography and image analysis. *Geoderma*, Volume 106, pp. 247-271.
- Please, J., 2011. *Individual Report I1*, Exeter: Exeter University.

- Robb, R., 1982. X-Ray Computed Tomography; From basic principles to application. *Ann. Rev. Biophys. Bioeng.*, Volume 11, pp. 177-201.
- Scheidegger, A., 1960. *The Physics of Flow through Porous Media*. 2nd ed. Toronto: University of Toronto Press.
- Sensen, C. & Hallgrímsson, B., 2009. *Advanced Imaging in Biology and Medicine*. Berlin: Springer-Verlag.
- Sperry, J. & Peirce, J., 1995. A model for estimating the hydraulic conductivity of granular material based on grain shape, grain size, and porosity. *Ground Water*, 33(6), pp. 892-898.
- Tobis, J., 2000. Influence of bed geometry on its frictional resistance under turbulent flow conditions. *Chemical Engineering Science*, Volume 55, pp. 5359-5366.
- Vontobel, P., Lehmann, E. & Carlson, W., 2005. Comparison of X-ray and Neutron Tomography Investigations of Geological Materials. *IEEE Transactions on Nuclear Science*, Volume 52.
- Whitehurst, L., 2012. *Individual Report (I2)*, Exeter: Exeter University.
- Winkler, B. et al., 2002. Neutron imaging and neutron tomography as non-destructive tools to study bulk-rock samples. *European Journal of Mineralogy*, Volume 14, pp. 349-354.
- X-Tek Xray Systems, 2006. *X-Tek XRay Systems Product Page*. [Online] Available at: <http://www.xtekxray.com/products/systems> [Accessed October 2011].
- Ziolkowska, I. & Ziolkowska, D., 1988. Fluid Flow inside Packed Beds. *Chemical Engineering Process*, Volume 23, pp. 137-164.

Appendices

Appendix A

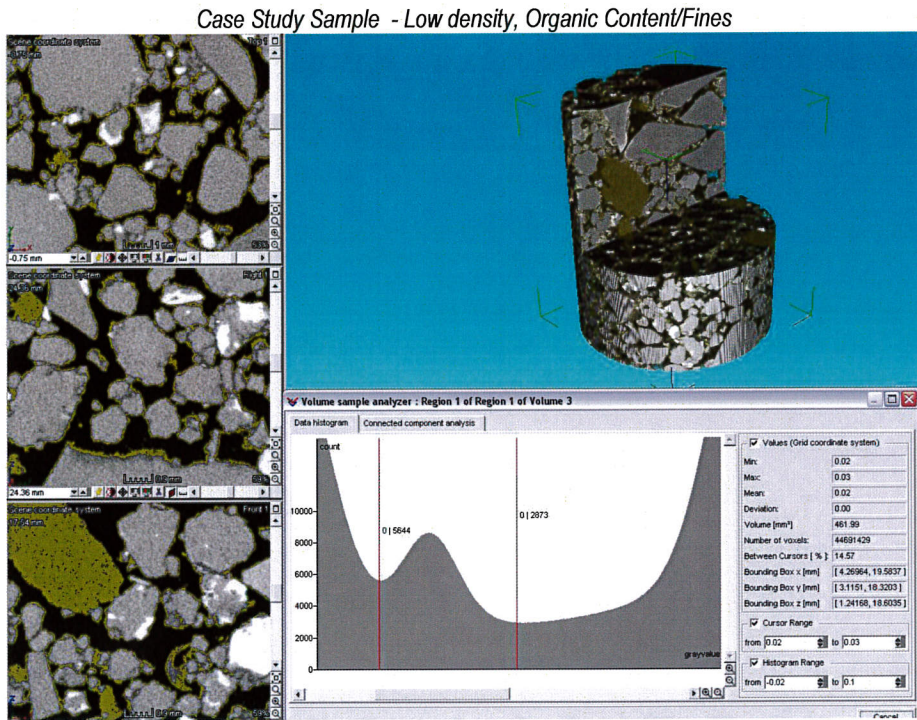


Figure 21 - Segmentation of low density region; Organic/Fines (Case Study)



Figure 22 - Isolated volume-rendered image of low density region; Organic/Fines (Case Study)

Case Study Sample - Highdensity, Gravel/Coarse Sand

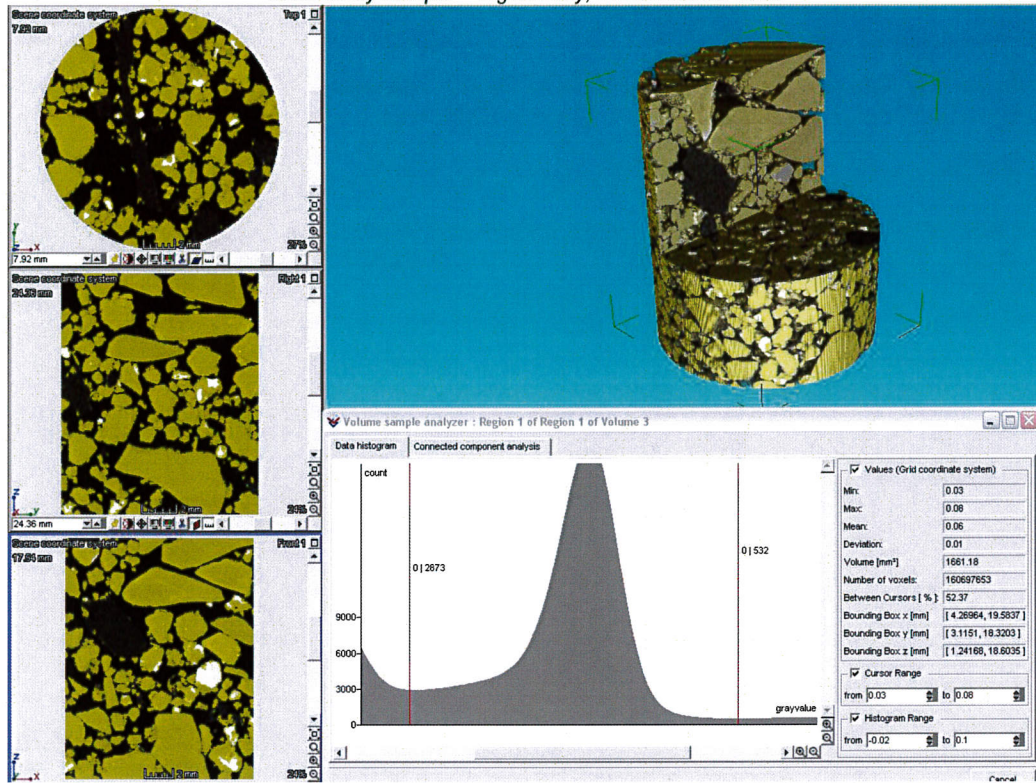


Figure 23 - Segmentation of high density region; Gravel/Coarse Sand content (Case Study)

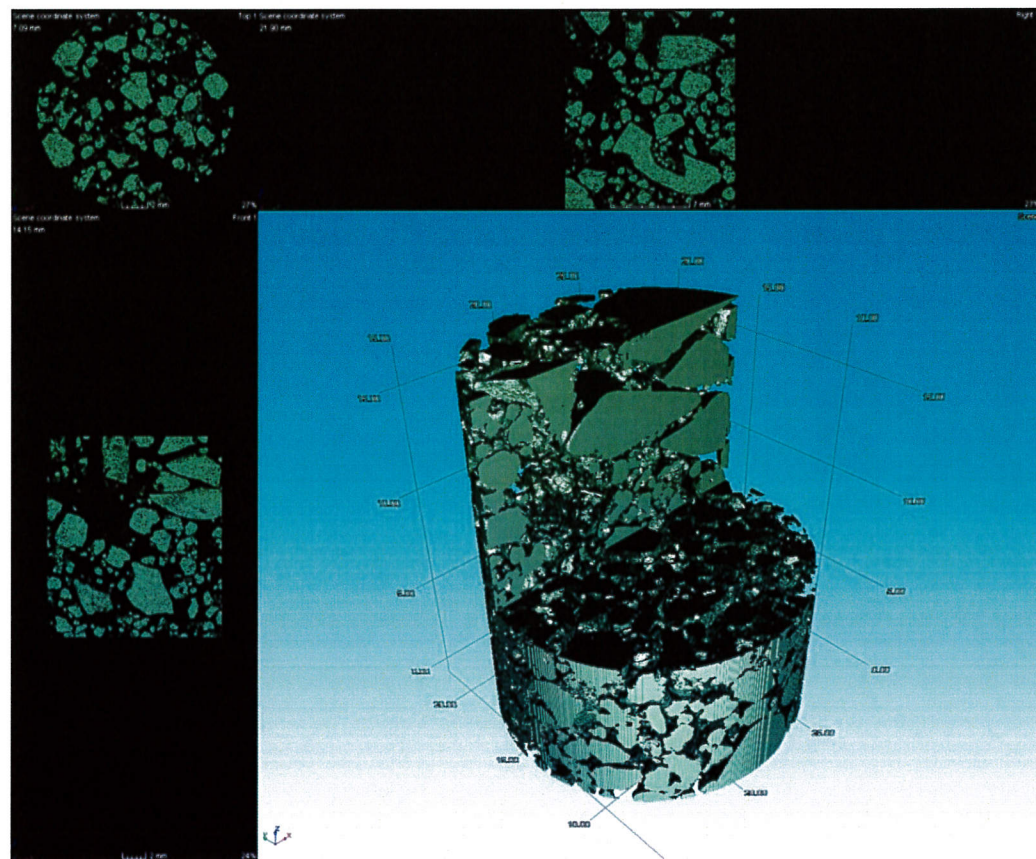


Figure 24 - Isolated volume-rendered image of high density region; Gravel/Coarse Sand (Case Study)

Case Study Sample – Combined model of segmented image regions

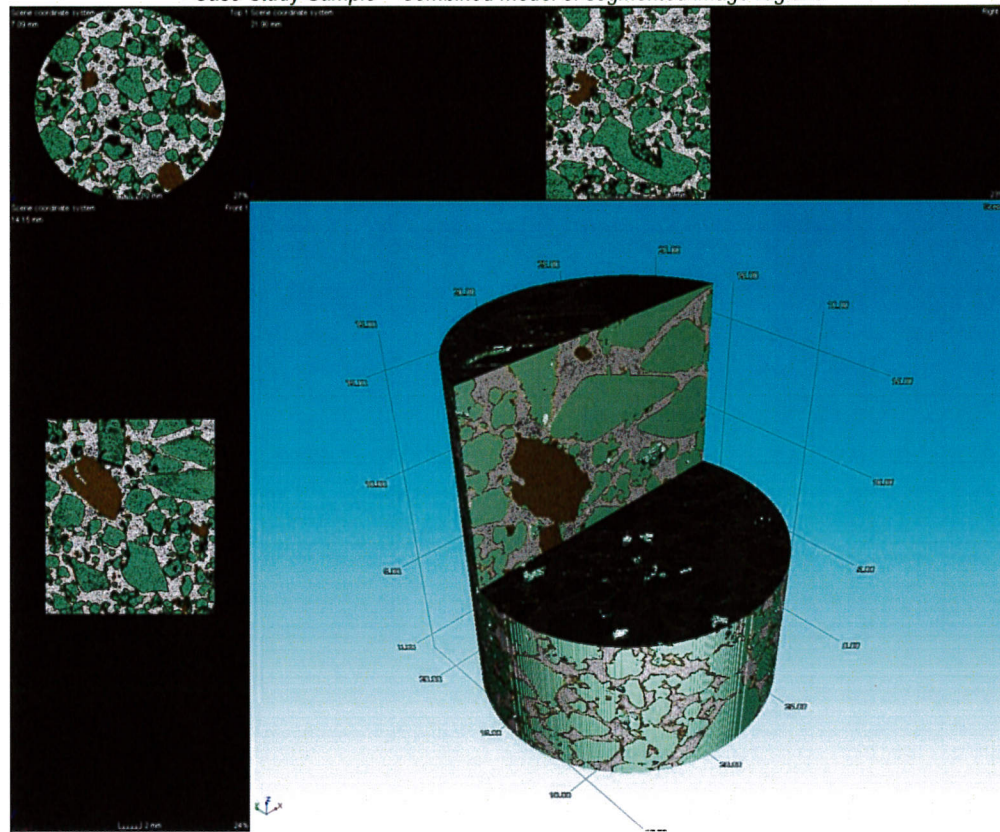


Figure 25 - Volume-rendered image of pore, low and high density regions (pore:white, low:gold, high: green) (Case Study)

Hydro Lab Sample - Low density, Organic Content/Fines

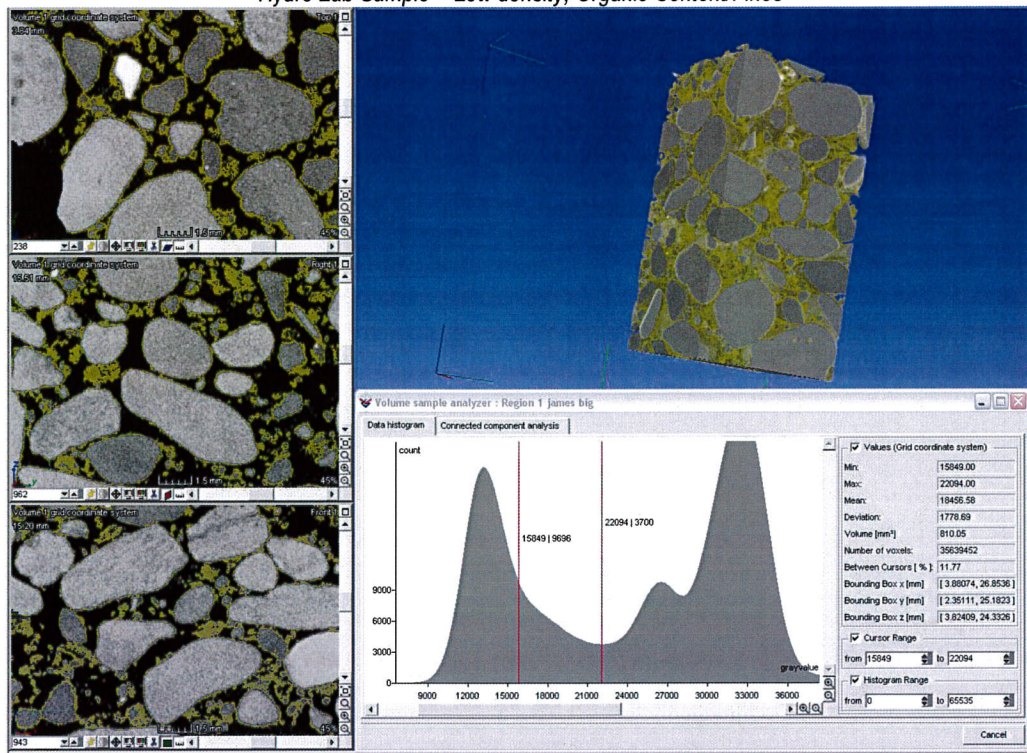


Figure 26 - Segmentation of low density region; Organic/Fines (Hydro Lab)

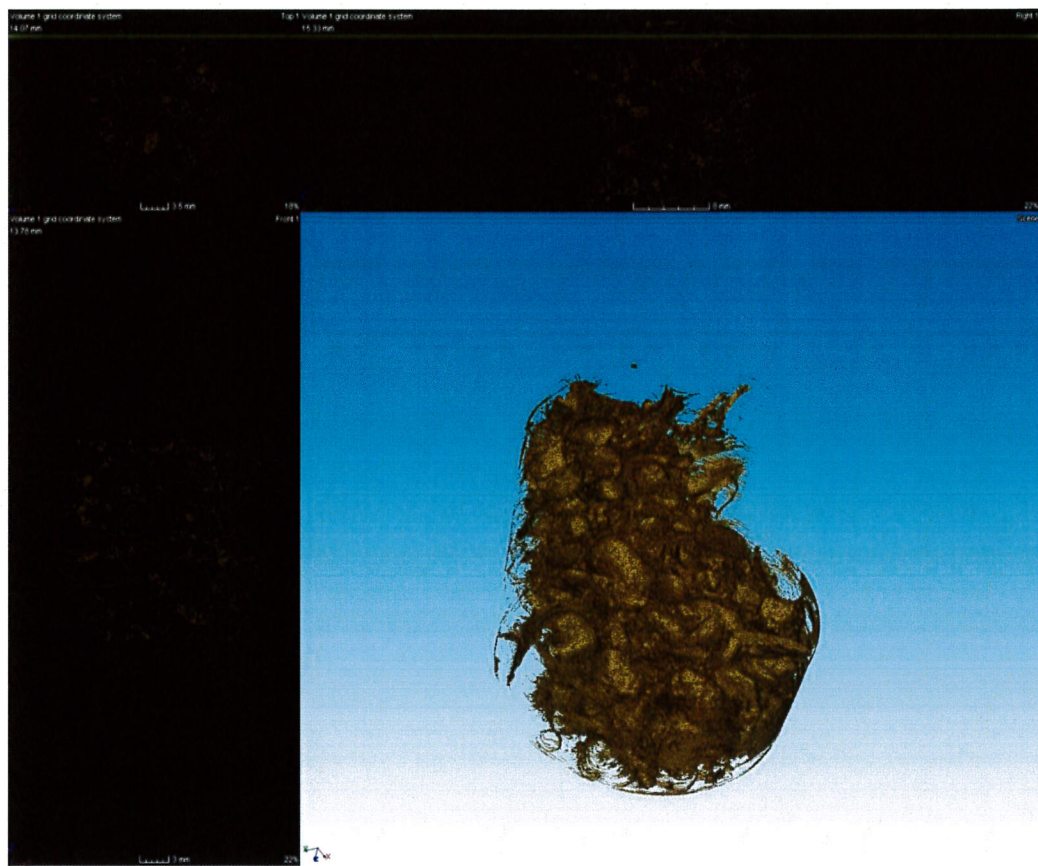


Figure 27 - Isolated volume-rendered image of low density region; Organic/Fines (Hydro Lab)

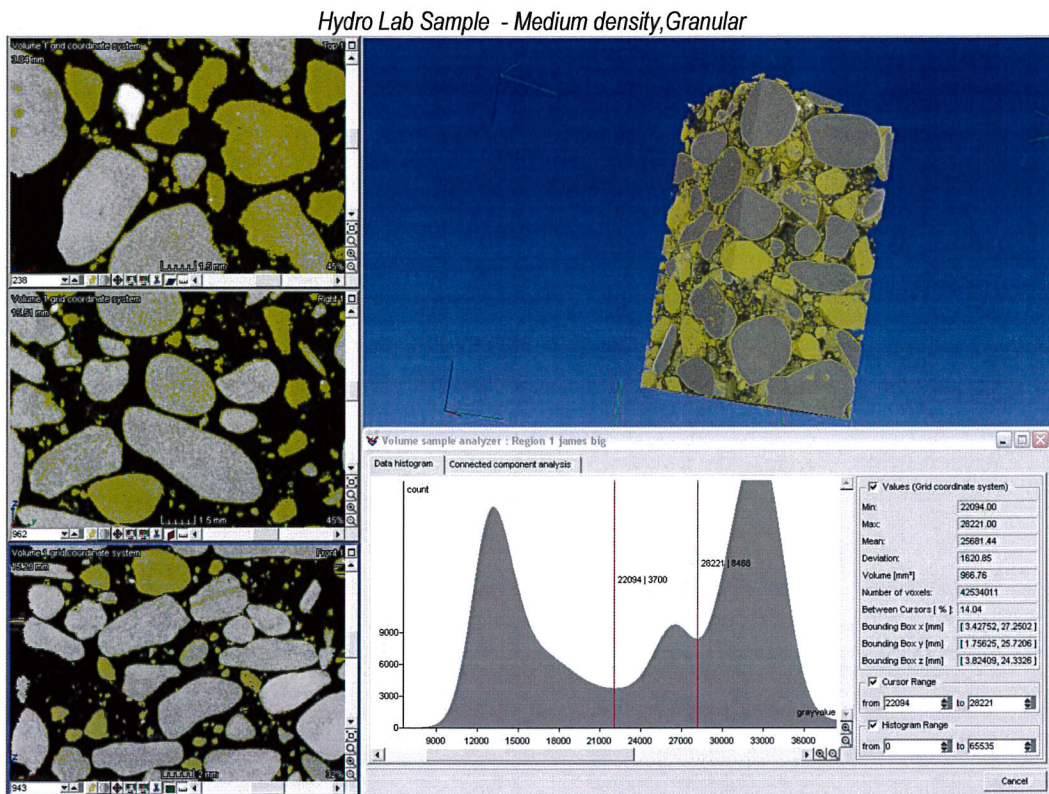


Figure 28 - Segmentation of medium density region (Hydro Lab)

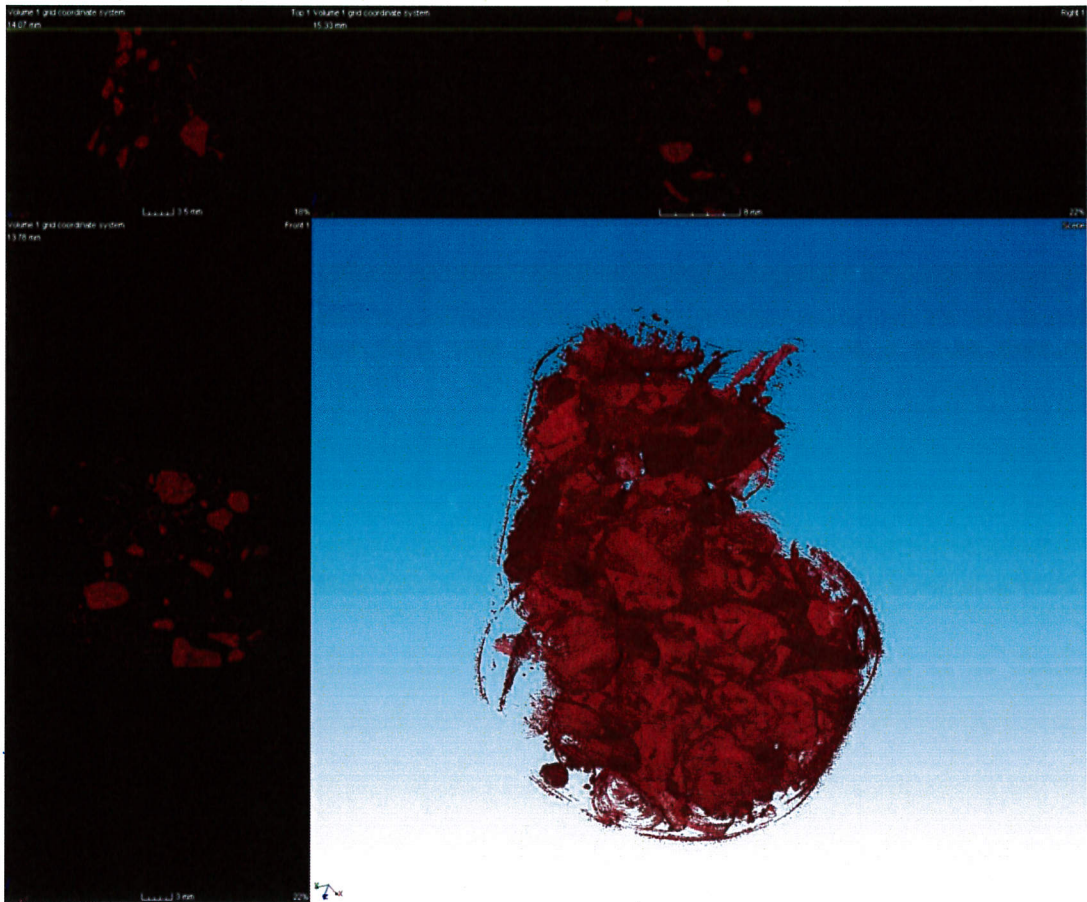


Figure 29 - Isolated volume-rendered image of medium density region (Hydro Lab)

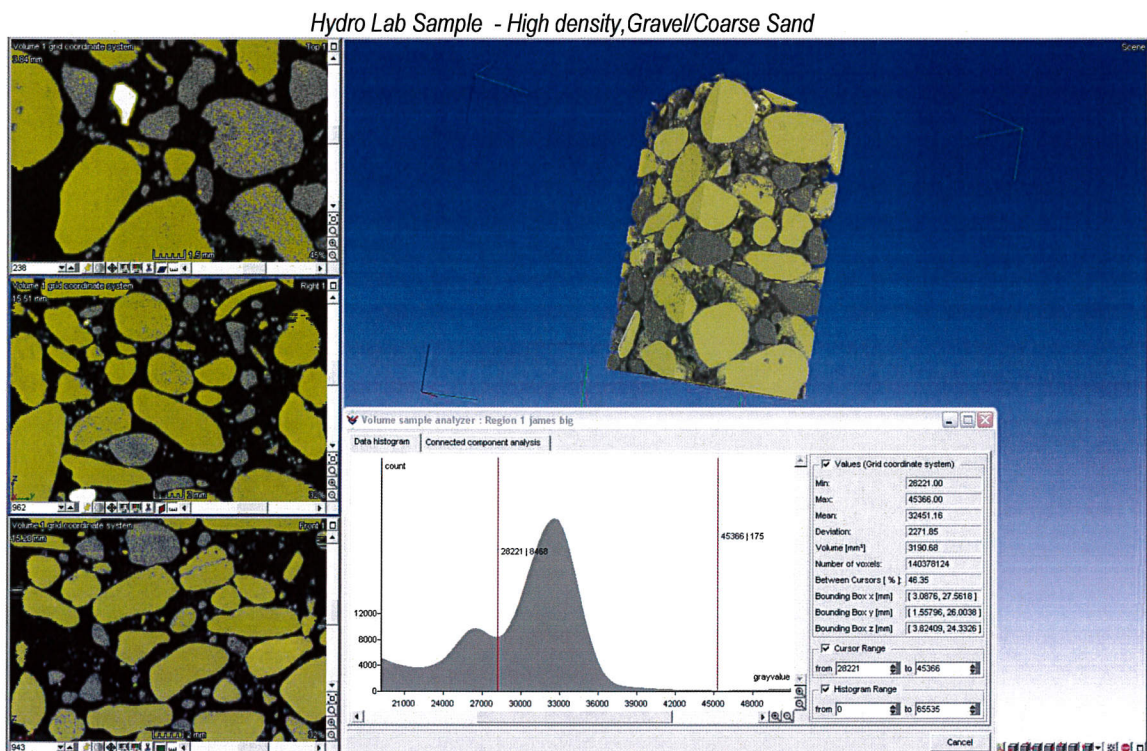


Figure 30 - Segmentation of high density region (Hydro Lab)

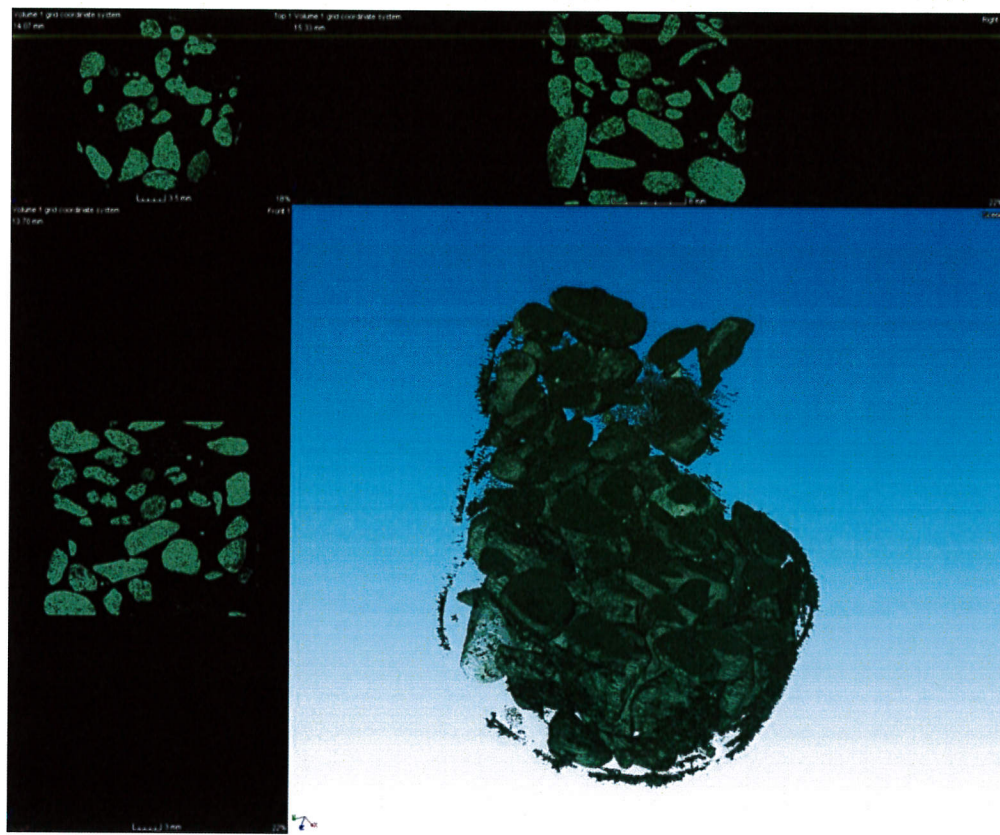


Figure 31 - Isolated volume-rendered image of high density region (Hydro Lab)

Case Study Sample – Combined model of segmented image regions

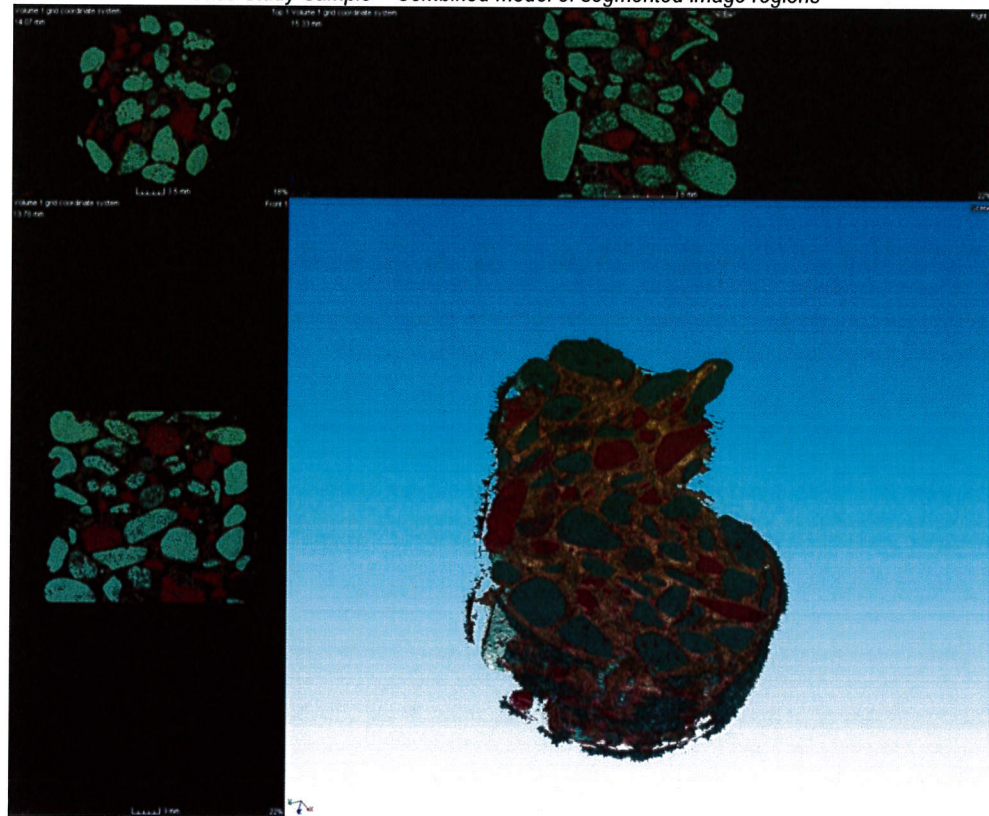


Figure 32 - Volume-rendered image of low, medium and high density regions (low:gold, medium: red, high:green)

Appendix B



Figure 33 – Samples used in initial scanning phase – Ref. section 5.1.2



Figure 34 - 'Hydro Lab' and 'Case Study' Samples

Appendix C

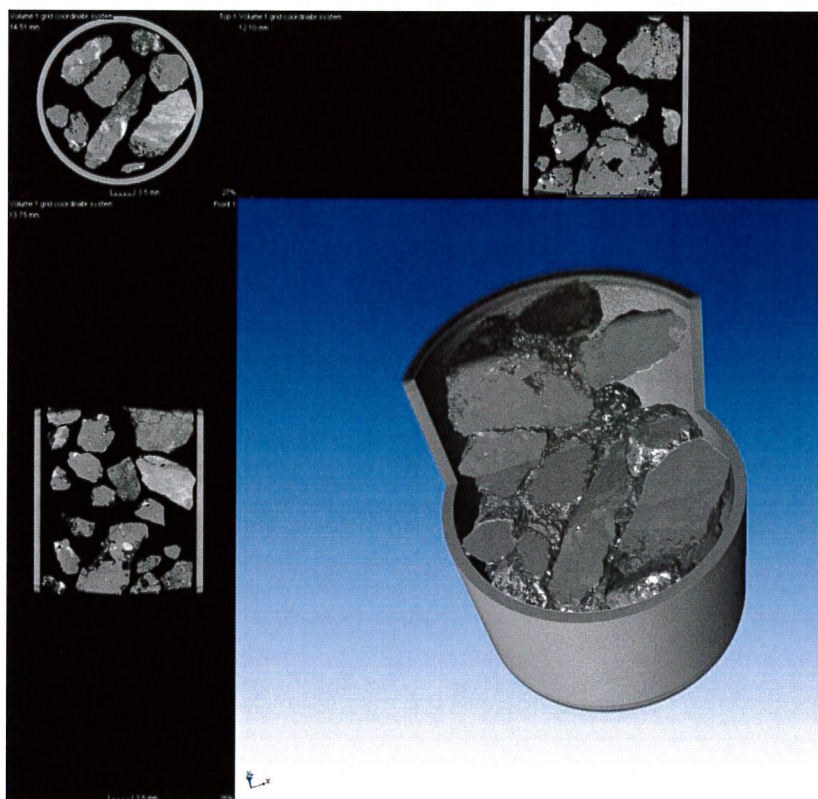


Figure 35 - Initial Scan Results - Coarse Gravel

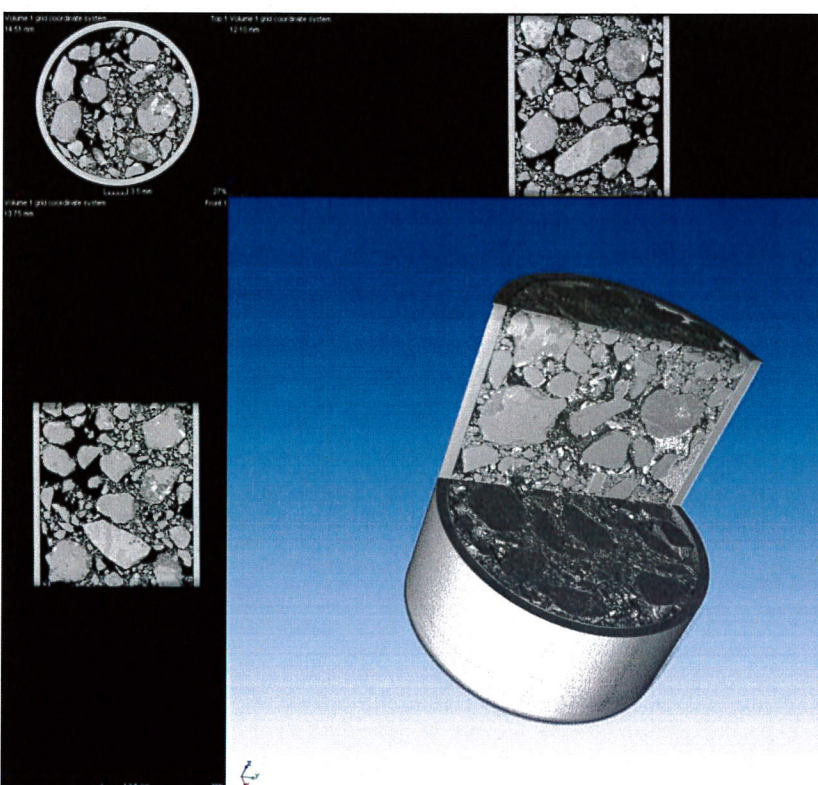


Figure 36 - Initial Scan Results - Fine Gravel

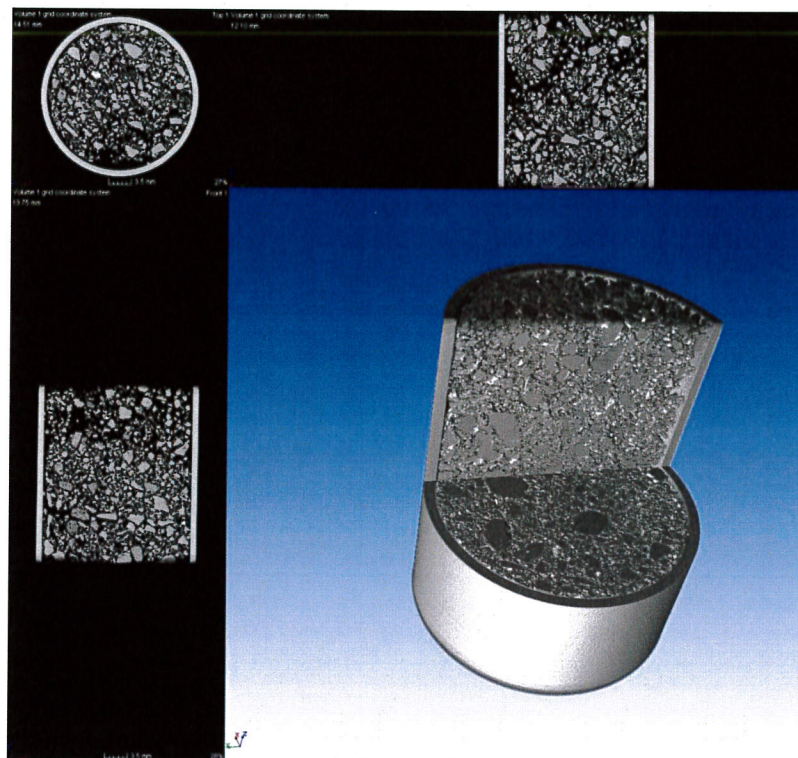


Figure 37 - Initial Scan Results – Sand

Appendix D

Table 5 - Sieve Testing Results

Hydro International Lab Sample	Sieve Size (mm)	Total Mass (g)	Sieve Mass (g)	Soil Mass (g)	% retained	cumul % retained	% pass through
	5	445.44	390.31	55.13	12.42898368	12.42898368	87.57101632
	2.36	696.83	405.03	291.8	65.78591397	78.21489765	21.78510235
	1.6	434.03	379.03	55	12.39967535	90.614573	9.385427
	1.18	359.44	352.32	7.12	1.605194337	92.21976734	7.780232663
	0.6	337.21	314.95	22.26	5.018486789	97.23825413	2.761745874
	0.425	295.03	291.84	3.19	0.719181171	97.9574353	2.042564704
	0.3	289.02	283.92	5.1	1.149788078	99.10722337	0.892776625
	tray	243.77	242.85	0.92	0.207412751	99.31463613	0.685363874
Totals				440.52	99.31463613		
Case Study Field Sample	Sieve Size (mm)	Total Mass (g)	Sieve Mass (g)	Soil Mass (g)	% retained	cumul % retained	% pass through
	5	738.12	390.31	347.81	27.88056112	27.88056112	72.11943888
	2.36	671.26	405.03	266.23	21.34108216	49.22164329	50.77835671
	1.6	576.21	379.03	197.18	15.80601202	65.02765531	34.97234469
	1.18	500	352.32	147.68	11.83807615	76.86573146	23.13426854
	0.6	502.86	314.95	187.91	15.06292585	91.92865731	8.071342685
	0.425	326.34	291.84	34.5	2.765531062	94.69418838	5.305811623
	0.3	310.8	283.92	26.88	2.154709419	96.8488978	3.151102204
	tray	280.02	242.85	37.17	2.979559118	99.82845691	0.171543086
Totals				1245.36	99.82845691		

Filterra USA Sample	Sieve Size (mm)	Total Mass (g)	Sieve Mass (g)	Soil Mass (g)	% retained	cumul % retained	% pass through
	5	392.11	390.31	1.8	0.382628659	0.382628659	99.61737134
	2.36	641.1	405.03	236.07	50.18174861	50.56437727	49.43562273
	1.6	525.49	379.03	146.46	31.13321854	81.69759582	18.30240418
	1.18	412.71	352.32	60.39	12.83719151	94.53478732	5.465212678
	0.6	337.14	314.95	22.19	4.716961078	99.2517484	0.7482516
	0.425	292.26	291.84	0.42	0.08928002	99.34102842	0.658971579
	0.3	284.19	283.92	0.27	0.057394299	99.39842272	0.60157728
	tray	244.42	242.85	1.57	0.333737219	99.73215994	0.267840061
	Totals			469.17	99.73215994		

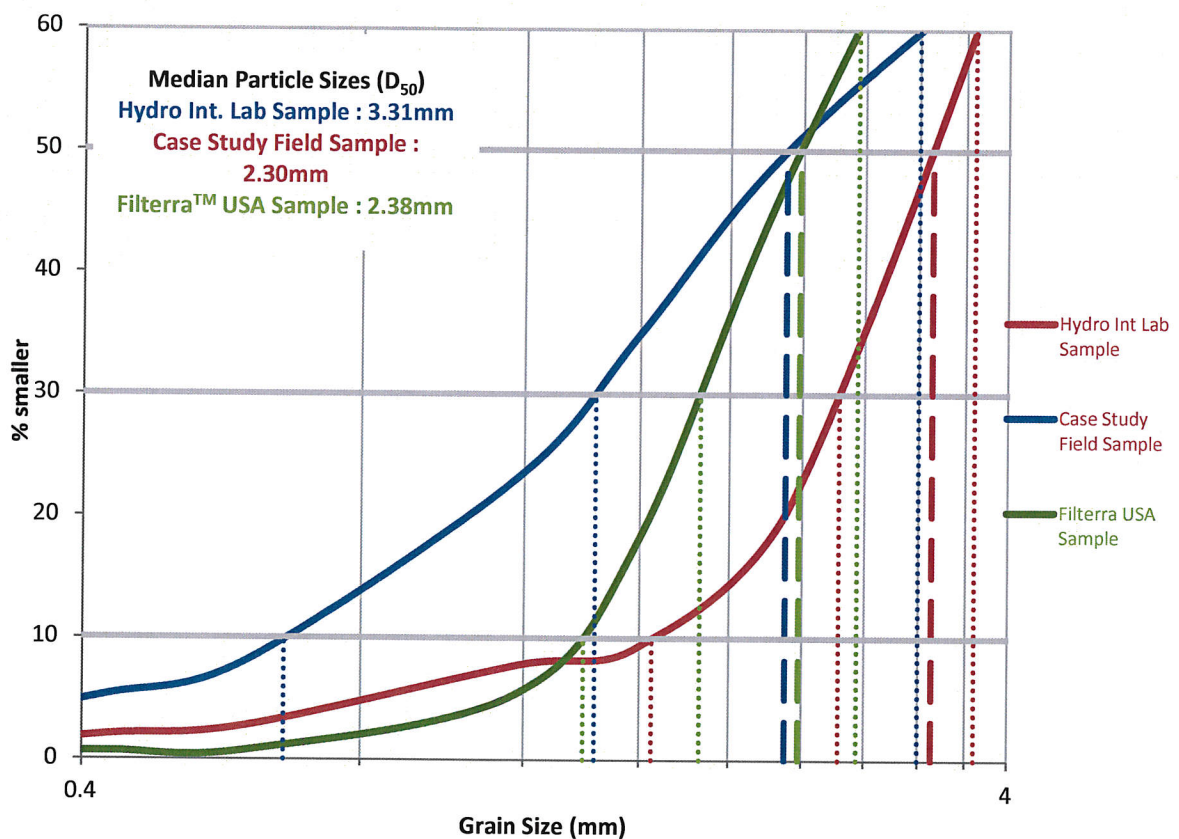


Figure 38 – Zoomed view of PSD from Sieve Analysis – Ref. section 6.3

Appendix E



Figure 39 - EOS Formiga P 100 - ALM Machine used to produce models



Figure 40 - Packed Bed Sample used in Flow Tests (Baker, et al., 2011) – 100mm x 100mm



Figure 41 - Experimental Apparatus for Flow Tests

Data collected from flow tests is available upon request, please contact author to request full data sets

Appendix F

Hazard/Risk Assessment Proforma

Project:	Investigating Stormwater Filters and Bioretention Systems	Risk Assessment No:	Ref 1	Review Dates:	1 st day of every even month
Operation/Task:	Experimental Procedures	Method Statement Title:	Experiment Stages		
Location/Area:	CT Lab, Fluids Lab, Structures Lab	Method Statement No:	Phases 2-9		

CATEGORY OF PERSONS AT RISK AND MEANS OF BRIEFING

CATEGORY OF PERSONS			Means of Briefing		
			RA	FCS	Other
Occupations involved in Activity (Specify):	JP				
Others Persons at Work (Specify):	LW				

Item	Activity	Hazards/Risks Identified	Risk Rating			Control Measures	Residual Risk			Responsibility	Monitoring Responsibility
			S	L	RR		S	L	RR		
1	Micro-CT scanning of soil samples	X-Ray Exposure	1	2	2	Operation of equipment restricted to trained operative (D.L. Wears). Machine has built in measures to prevent x-ray exposure	1	1	1	James Please	James Please
2	Flow Tests	Working at height	2	3	6	Clear working area, safe use of ladder(s)	2	1	2	James Please	James Please

K S = Severity Rating L = Likelihood of Occurrence RR = Risk Rating 1
E Y:
Y:
1. Negligible 1. Improbable 5. Unacceptable risk, plan out or add further controls
2. Minor Injury 2. Remote 1 - 10% 4. Acceptable only if no other method viable and with high level controls in place
3. Major Injury (RIDDOR) 3. Possible 10 - 50% 3. Acceptable with suitable controls
4. Fatality 4. Probable 50 - 90% 2. Acceptable, no further action required
5. Multiple Fatality 5. Almost certain 90%+ 1
RA Prepared by (Name): JAMES PLEASE Signature: Date: November 2011
RA Prepared Approved by (Name): Signature: Date:

Figure 42 - Risk Assessment for Experimental Procedures

Hazard/Risk Assessment Proforma

Project:	Investigating Stormwater Filters and Bioretention Systems	Risk Assessment No:	Ref 2	Review Dates:	1 st day of every even month
Operation/Task:	Site Visit	Method Statement Title:	Group Site Visit		
Location/Area:	Barry, South Wales	Method Statement No:	Phase 4		

CATEGORY OF PERSONS AT RISK AND MEANS OF BRIEFING

CATEGORY OF PERSONS			Means of Briefing		
			RA	FCS	Other
Occupations involved in Activity (Specify):	AB				
Others Persons at Work (Specify):	SP				
	JP				
	SR				
	JT				
	LW				
	SW-G				
	DJ				

Item	Activity	Hazards/Risks Identified	Risk Rating			Control Measures	Residual Risk			Responsibility	Monitoring Responsibility
			S	L	RR		S	L	RR		
1	Site Visit	Active Car Park, under constant use	3	2	6	High-Vis Jackets worn by all, care and diligence at all times	1	1	1	James Please	James Please
2	Extraction of Sample	Heavy steel grating, lifting	2	2	4	Lifting and removal of grating conducted by only Daniel Jarman (wearing appropriate PPE)	1	1	1	Daniel Jarman	James Please

K S = Severity Rating L = Likelihood of Occurrence RR = Risk Rating 1
E Y:
Y:
1. Negligible 1. Improbable 5. Unacceptable risk, plan out or add further controls
2. Minor Injury 2. Remote 1 - 10% 4. Acceptable only if no other method viable and with high level controls in place
3. Major Injury (RIDDOR) 3. Possible 10 - 50% 3. Acceptable with suitable controls
4. Fatality 4. Probable 50 - 90% 2. Acceptable, no further action required
5. Multiple Fatality 5. Almost certain 90%+ 1
RA Prepared by (Name): JAMES PLEASE Signature: Date: November 2011
RA Prepared Approved by (Name): Signature: Date:

Figure 43 - Risk Assessment for Site Visit